# An Experimental Investigation of Reactive, Turbulent, Recirculating Jet Mixing

G. D. Smith and T. V. Giel
ARO, Inc.

May 1980

Final Report for Period October 1977 — February 1979

# ARNOLD ENGINEERING DEVELOPMENT CENTER
# ARNOLD AIR FORCE STATION, TENNESSEE
# AIR FORCE SYSTEMS COMMAND
# UNITED STATES AIR FORCE

This report has been reviewed by the Office of Public Affairs (PA) and is releasable to the National Technical Information Service (NTIS). At NTIS, it will be available to the general public, including foreign nations.
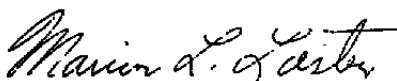
**APPROVAL STATEMENT**

This report has been reviewed and approved.

ELTON R. THOMPSON
Project Manager
Directorate of Technology

Approved for publication:

FOR THE COMMANDER

MARION L. LASTER
Director of Technology
Deputy for Operations

# UNCLASSIFIED

| REPORT DOCUMENTATION PAGE | | READ INSTRUCTIONS BEFORE COMPLETING FORM |
|---|---|---|
| 1 REPORT NUMBER<br>AEDC-TR-79-79 | 2 GOVT ACCESSION NO. | 3 RECIPIENT'S CATALOG NUMBER · |
| 4 TITLE (and Subtitle)<br>AN EXPERIMENTAL INVESTIGATION OF REACTIVE, TURBULENT, RECIRCULATING JET MIXING | | 5 TYPE OF REPORT & PERIOD COVERED<br>Final Report, Oct. 1977 – Feb. 1979 |
| | | 6 PERFORMING ORG REPORT NUMBER |
| 7 AUTHOR(s)<br>G. D. Smith and T. V. Giel, ARO, Inc., a Sverdrup Corporation Company | | 8 CONTRACT OR GRANT NUMBER(s)<br>PO-79-00002 |
| 9 PERFORMING ORGANIZATION NAME AND ADDRESS<br>Arnold Engineering Development Center/DOT<br>Air Force Systems Command<br>Arnold Air Force Station, TN 37389 | | 10. PROGRAM ELEMENT, PROJECT, TASK AREA & WORK UNIT NUMBERS<br>Program Element 61102F<br>Project Number 2308/A2 |
| 11 CONTROLLING OFFICE NAME AND ADDRESS<br>Air Force Office of Scientific Research/NA<br>Building 410<br>Bolling Air Force Base, DC 20332 | | 12. REPORT DATE<br>May 1980 |
| | | 13 NUMBER OF PAGES<br>72 |
| 14 MONITORING AGENCY NAME & ADDRESS(If different from Controlling Office) | | 15 SECURITY CLASS (of this report)<br>UNCLASSIFIED |
| | | 15a DECLASSIFICATION/DOWNGRADING SCHEDULE N/A |

16 DISTRIBUTION STATEMENT (of this Report)

Approved for public release; distribution unlimited.

17 DISTRIBUTION STATEMENT (of the abstract entered in Block 20, If different from Report)

18 SUPPLEMENTARY NOTES

Available in Defense Technical Information Center (DTIC).

19 KEY WORDS (Continue on reverse side if necessary and identify by block number)

dump combustors      experimental data
jet mixing      turbulence/chemistry interactions
recirculation
turbulent mixing
laser velocimeter

20 ABSTRACT (Continue on reverse side if necessary and identify by block number)

'An experimental investigation of ducted, two-stream, subsonic, turbulent jet mixing with recirculation was conducted. A primary jet of air at a mass flow rate of 0.580 lbm/sec and bulk velocity of 335 ft/sec was surrounded by an outer hydrogen stream at a mass flow rate of 0.002 lbm/sec and bulk velocity of 3 ft/sec (overall equivalence ratio of 0.12). The ratio of the duct to inner nozzle diameter was 2.5. Radial distributions of mean axial and radial

DD FORM 1473   1 JAN 73   EDITION OF 1 NOV 65 IS OBSOLETE

# UNCLASSIFIED

20.   ABSTRACT, Concluded.

velocity, axial and radial turbulence intensity, velocity cross
correlation, gas composition, static temperature, and total
pressure, as well as axial distribution of wall static pressure,
are presented for axial stations from zero to six duct diameters
from the nozzle exit plane, both with and without chemical
reactions.   The maximum turbulent intensities which occurred in
the center of the mixing layer and within the recirculation eddy
were very high, having values in excess of 20 percent of the jet
exit velocity.   The data clearly indicate that the mixing is slower
in the chemically reactive flow field than in the nonreactive flow
field and that the presence of chemical reactions had a significant
effect on the size and location of the recirculation zone within
the mixing duct.

AFSC
Arnold AFS Tenn

## PREFACE

# CONTENTS

# ILLUSTRATIONS

## 1.0 INTRODUCTION

Recirculating flow fields established by turbulent jet mixing of two coaxial streams in a constant-area, axisymmetric duct occur in many industrial and aerospace burner, furnace, and combustor configurations. The so-called "sudden" expansion or "dump" combustors used in ramjet-rocket propulsion systems are designed on the principle of establishing and maintaining combustion in regions of recirculating flow within the combustor. Historically, combustors have been designed by "cut and try" methods. While such methods have led to practical and thermodynamically efficient combustors, they are time-consuming and expensive. More recently, systems have been encountered in which the design criteria cannot be pragmatically achieved by purely experimental means. The ability to deal with such advanced systems problems requires detailed knowledge of both the fluid mechanical processes and the coupling between the turbulent flow and the chemical reactions.

The purpose of the study reported herein was to obtain data to aid in the development and evaluation of analytical techniques to analyze and predict the turbulent mixing and combustion phenomena which occur in a wide variety of engineering applications. This development requires data on many different flow configurations if the techniques are to be general and applicable to more than a limited number of configurations. Experimental data are available for boundary-layer-type flow, but development and evaluation of analytical models for ducted, recirculating flow configurations has been hampered by the lack of detailed experimental flow-field information for such configurations.

Radial distributions of total pressure, mean axial and radial velocity, turbulence intensity, gas composition, velocity cross-correlation, static temperature, and wall static pressure distributions were obtained in a confined, axisymmetric, recirculating flow field typical of a dump combustor. The measurements were obtained both with and without chemical reactions at one fixed stoichiometry. The data may be used as a guide for design estimates for combustors or combustion processes and as an aid in developing and evaluating theoretical models and predictive techniques for such flows and processes. The data are tabulated in Appendix A.

The essential features of the recirculating flow field are shown in Fig. 1. For a certain range of fluid influx conditions, jet mixing of coaxial streams leads to the creation of an eddy of recirculating fluid existing on a time-averaged basis as a toroidal, highly vortical region with high turbulent intensities and relatively low average velocities. The eddy of the recirculating region is generated when the "entrainment or pumping

5

capacity" of the higher velocity, primary jet stream is greater than the mass flow available in the outer, lower velocity, secondary stream. For those conditions, the primary jet "establishes" the recirculation eddy which provides mass flux to balance the jet entrainment requirements. The recirculation eddy can exist with or without secondary flow. However, as the secondary mass flow rate is increased to some critical "blow-off" value with a constant primary jet mass flow rate, the recirculation eddy structure disappears and the duct flow becomes characterized by positive axial velocities throughout the flow. The pertinent features which may be used to describe the time-averaged flow field with recirculation are as follows:

1.  the axial location of the characteristic time-averaged stagnation points on the duct wall, denoted $X_{FS}$ and $X_{RS}$ in Fig. 1;

2.  the time-averaged axial velocity field;

3.  the time-averaged distribution of mass, energy, or temperature of the fluid from the primary stream which characterizes the qualitative and quantitative nature of the mixing that has occurred between the two streams;

4.  the time-averaged axial distribution of wall static pressure.
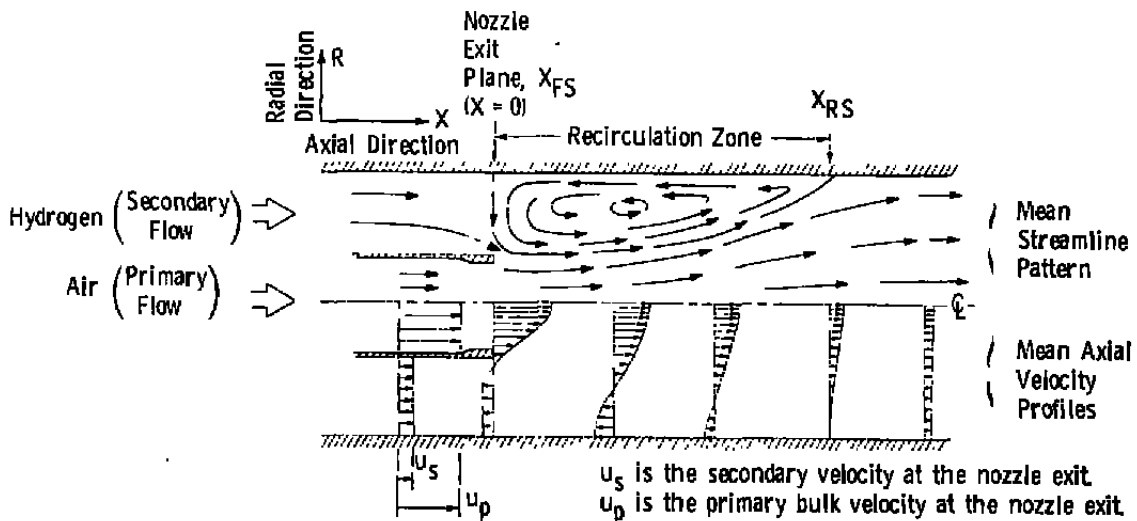


Figure 1. Features of turbulent, ducted mixing flow field
with recirculation.

All of these gross features of the flow, their spatial distributions and magnitudes, appear from experimental evidence to be dependent on the ratios ($u_s/u_p$, $\rho_s/\rho_p$, $R_s/R_p$),

6

on a Reynolds number based on the primary flow at the nozzle exit station, and on chemical reactions occurring in the flow. However, it is also an empirical observation that for sufficiently high values (> 1.5 x 10⁴) of the primary jet Reynolds number, defined by

$$N_{Re_p} = \rho_p u_p R_p / \mu_p \tag{1}$$

the time-averaged velocity, species concentration, and static pressure fields become independent of $N_{Re}$, which is the case in the present study.

## 2.0 APPARATUS

### 2.1 TEST CELL

The test cell, which is a modification of the one used by Schulz (Ref. 1) and Chriss (Ref. 2), is shown in Fig. 2. The test chamber consists of a 5-ft-long stainless steel duct with an inside diameter of 5.24 in. A hydraulically driven, axially traversing nozzle
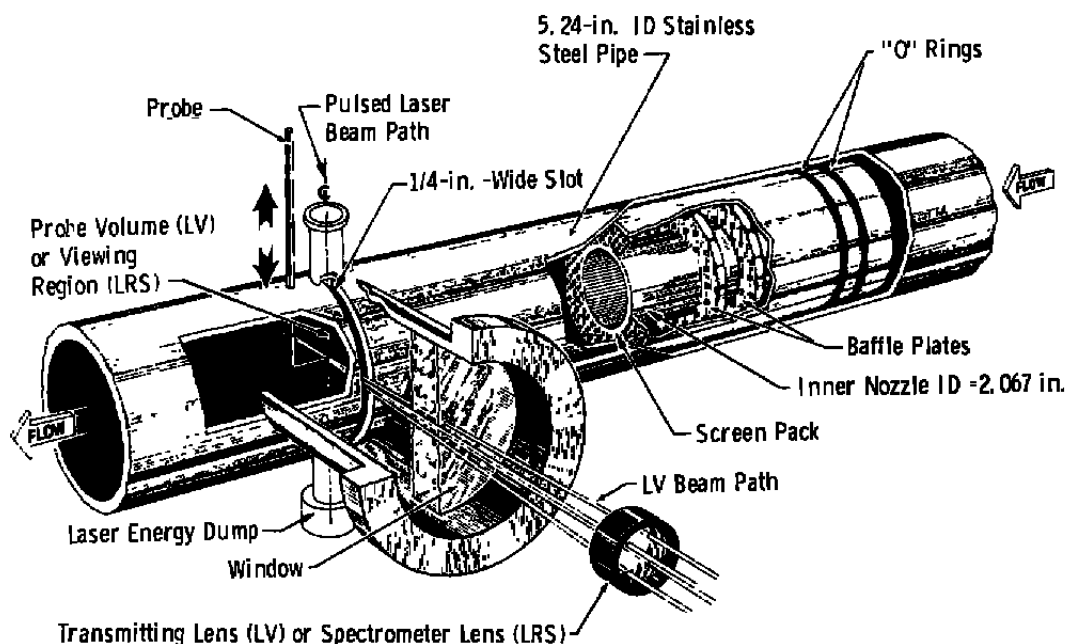


Figure 2. Recirculating flow combustor simulation facility.

assembly was mounted inside the duct. The nozzle assembly was traversed in discrete steps during the testing to vary the distance between the primary jet nozzle exit plane and the radially positionable pitot pressure and gas sampling probe. An O-ring system

7

provided a seal between the movable nozzle assembly and the duct. The test chamber included a 1/4-in.-wide slot centered at the axial plane of the traversing probe tip as shown in Fig. 2. The slot provided optical access for the laser instrumentation. A quartz window assembly was used to seal the slot, and an optical access port was located on top of the test cell in the measuring plane to allow passage of the pulsed laser beam required for the laser-Raman apparatus. A laser energy dump was located 180 deg from the optical access port to allow dissipation of the pulsed laser beam energy.

The primary nozzle assembly consisted of a 2.067-in.-ID circular pipe which introduced the primary air jet at a nominal bulk flow velocity of 335 ft/sec. An annular secondary injector assembly was provided through which hydrogen entered the duct. The secondary hydrogen flow passed through two porous plates and a screen pack, shown in Fig. 2, which acted to stabilize the flow system. External water spray nozzles were positioned outside the duct to cool the walls. A spark plug was located downstream of the traversing probe to ignite the combustible hydrogen-air mixture.

## 2.2 INSTRUMENTATION

### 2.2.1 Pressure and Temperature

A water-cooled total pressure and gas sampling probe of the type described in Ref. 3 was installed in the duct at a fixed axial position. The probe tip, detailed in Fig. 3, was traversed radially across the duct by a hydraulic drive mechanism. By changing the positions of the axially traversing nozzle assembly and the radially traversing probe, axial

Notes: 1. Not to Scale
2. ⇐=== Indicates Water Flow
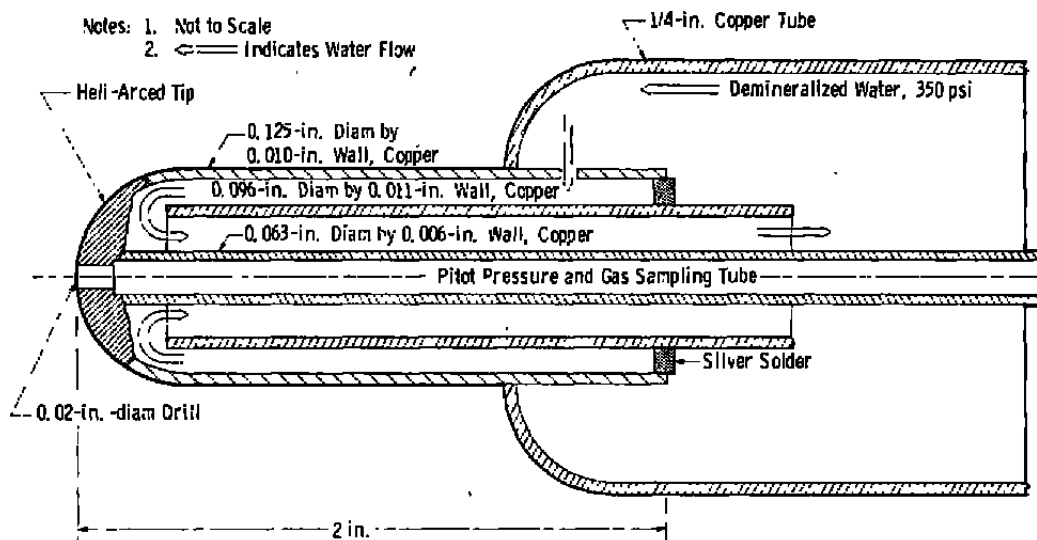
Figure 3. Water-cooled probe tip.

8

and radial surveys were made in the recirculating flow field. The total pressure was sensed with a variable capacitance transducer and a strain-gage transducer to obtain maximum accuracy over the range of pressure encountered.

In addition to the probe assembly, 41 static pressure orifices (0.040-in. diameter) were installed approximately 1 in. apart along the duct wall. The orifices were connected to a water manometer which was photographed during the tests to record the wall static pressure distribution.

The total temperature of the gaseous supplies of hydrogen and air were measured with copper-constantan thermocouples located upstream of critical-flow venturis, which were used to meter the primary and secondary mass flows.

### 2.2.2 Gas Concentration

The mass fraction of hydrogen present in the probe-extracted gas samples was measured using two different techniques. For the case of flow with no chemical reactions, extracted gas samples were analyzed using a thermal conductivity cell apparatus. The apparatus was similar to that described in Ref. 4 and was calibrated prior to each test period by passing known mixtures of $GH_2/GN_2$ through the cell and measuring millivolt output. For the case of flow with chemical reactions occurring, extracted gas samples were analyzed using an infrared emission-absorption cell apparatus similar to that described in Ref. 5. Gas samples were withdrawn from the stream through the probe and passed through a platinum-wound catalytic heater to insure completion of the chemical reaction. The sample was then drawn into an evacuated chamber which had an optical viewing port on each end (Fig. 4). The infrared emission-absorption apparatus was then used to determine the infrared transmissivity of the sampled gas, from which the water vapor mass fraction could be calculated using Beer's law (Ref. 5). The entire gas sampling system was steam heated to prevent condensation of the water vapor in the gas sample.

Additionally, for the case of flow with chemical reactions, species concentration and static temperature measurements were obtained using an in-situ laser-Raman spectroscopy apparatus which is described in detail in Ref. 6 and shown schematically in Fig. 5. A Q-switched ruby laser and a spectrometer were mounted on a traversing table as shown in Fig. 5. The pulsed ruby laser beam was transmitted vertically through the test section using a transmitting lens and mirror. The spectrometer viewing plane was oriented 90 deg from the path of the laser beam. Alignment of the optical apparatus and location of the spectrometer viewing path/laser beam intersection were determined with the aid of a He-Ne alignment laser. The spectrometer viewing volume was 0.039 in. in diameter by 0.125 in. long. Temperature and air number density were determined by analyzing the
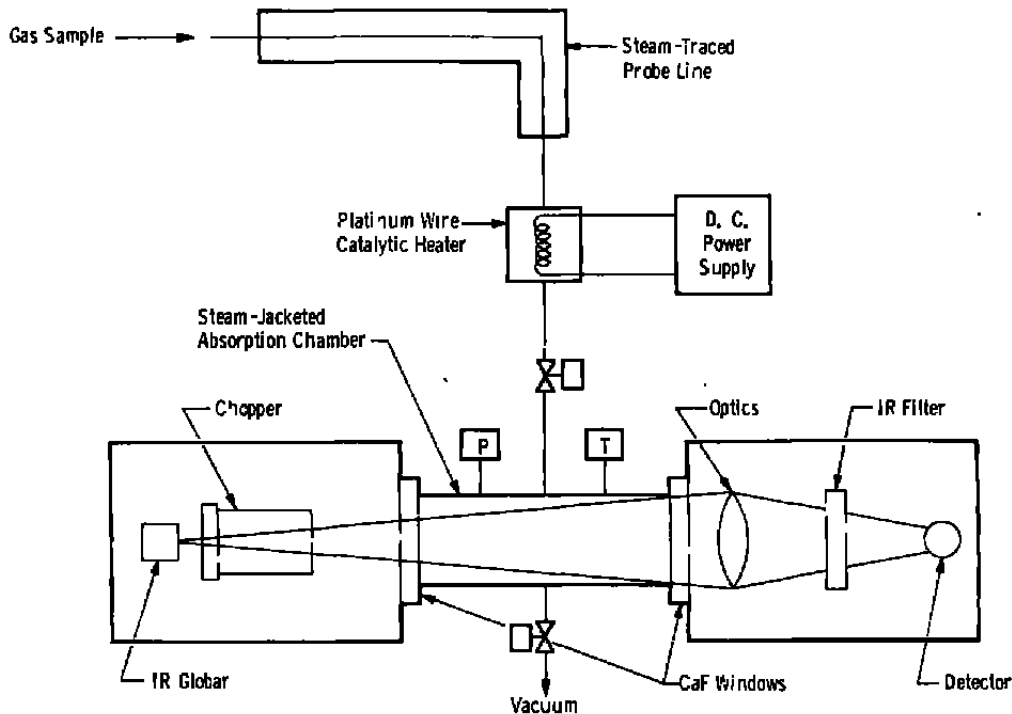
**Figure 4. Schematic of IR emission-absorption apparatus.**

pure rotational Raman lines as described in Ref. 6. Data were obtained by pulsing the ruby laser and measuring the intensity of the $N_2$-$O_2$ rotational Raman line, which is related to the rotational temperature of the gas and the molecular species number density. The laser pulse width was $20 \times 10^{-9}$ sec, and the experimental data rate was 15 pulses per data point at a rate of 15 pulses per minute. The low experimental data rate, resulting in a relatively low statistical confidence level, was necessitated by time constraints on testing. The results obtained for the mean temperature and species number density are, therefore, only approximations to the true value of these parameters. The degree of approximation can be evaluated in terms of the statistical confidence level (Ref. 7). For a data set of 15 samples and a 95-percent confidence level, the confidence interval for the mean temperature in the recirculating flow field is less than 20 percent.

## 2.2.3 Velocity and Turbulence

### 2.2.3.1 Selection of Velocity Measurement Technique

The presence of high temperatures, chemical reactions, recirculation, and high turbulence levels in the simulated dump combustor flow field precludes the accurate determination of flow characteristics by conventional methods. Conventional

instrumentation systems such as hot-wire anemometers and pitot probes materially interact with the flow environment and introduce local flow disturbances which make them unsuitable for recirculation flow measurements. Such devices are subject to damage because of impact and thermal loading. The pitot probe does not adequately respond to fluid transients and can be sensitive to changes in flow direction so that it is of little use in measurements of turbulence. Hot-wire anemometers can provide accurate turbulence information; however, they are limited to moderate turbulence levels, require an independent measurement of fluid temperature in a nonisothermal flow, and above all are fragile and incapable of survival in the hostile environment of a combustor flow field. These difficulties generally can be avoided by use of a laser velocimeter (LV) system which can, under controlled circumstances, obtain the required data with reasonable accuracy. It has been shown (Ref. 8) that concurrent determination of shear stress and turbulence intensity is possible if both axial and radial velocities are measured simultaneously with the LV system. In addition, a Bragg-diffracted LV will indicate the flow directionality in a recirculating flow. Thus a Bragg-diffracted LV was selected as the velocity-measuring instrument to be applied to the flow in the simulated dump combustor.
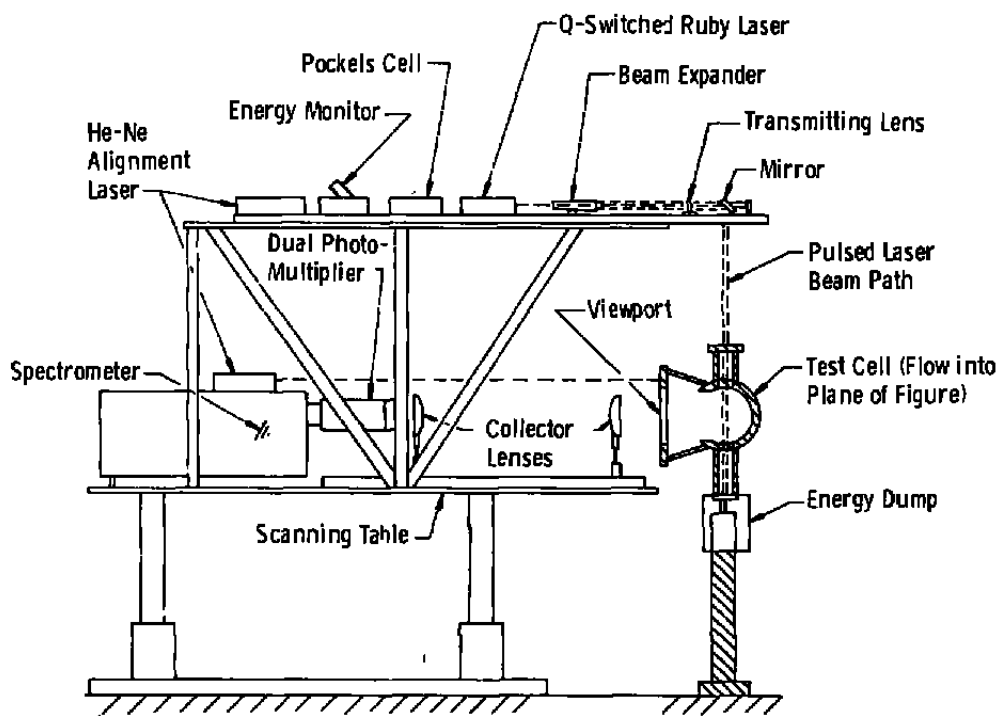


Figure 5.  Laser-Raman experimental configuration.

11

### 2.2.3.2 Laser Velocimeter

Velocity measurements were made in the duct with an off-axis, individual realization, two-component Bragg-diffracted laser velocimeter operating in the backscatter mode as shown in Fig. 6. An argon-iron laser capable of producing an optical power of 2 watts in the 514.5-nm wavelength line was the light source. Light from the laser is directed by mirrors and lenses which reorient and focus the beam at the center of a two-component Bragg cell beam splitter. The water-filled cell has 15- and 45-MHz piezoelectric oscillators in the horizontal and vertical branches, respectively. The two lower order beams for both the horizontal and vertical beam splits were allowed to pass through a collimating lens and a beam expander. The resulting parallel beams were then redirected by mirrors and lenses and focused together in the flow field. In the beam crossover region, or probe volume, a set of interference fringes is formed, the dominant fringe pair being aligned with the longitudinal and vertical axes of the flow field. Since the Bragg cell imparts to each higher order beam a frequency shift equal to the
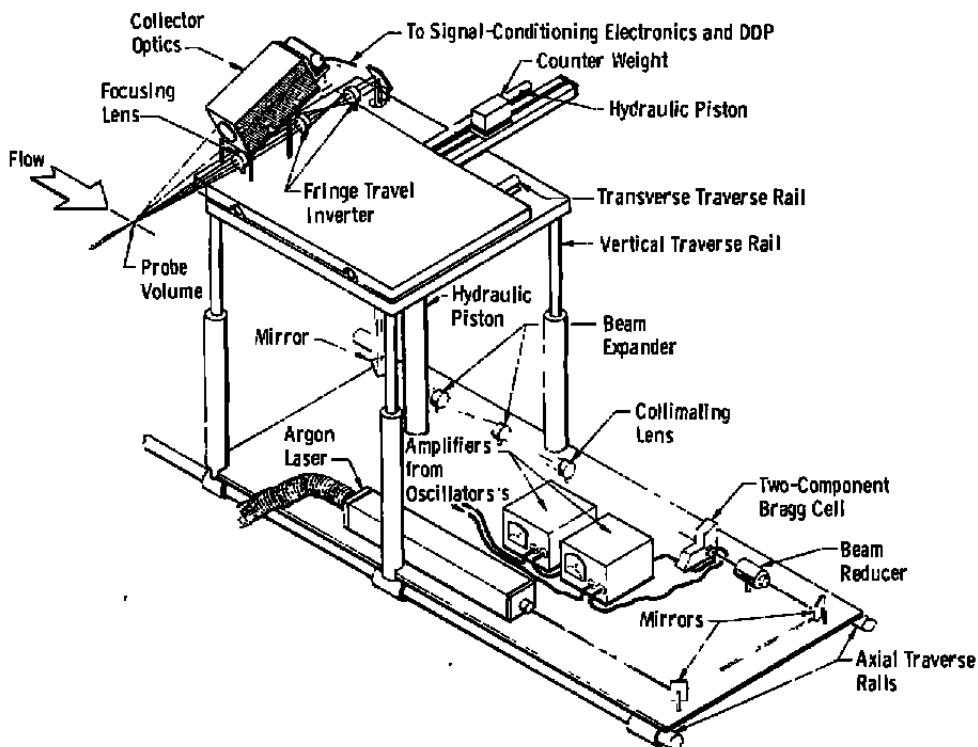


**Figure 6. Laser velocimeter and traverse system.**

piezoelectric oscillator frequencies, the fringes are not stationary but move at a reference velocity proportional to the frequency of the ultrasonic drivers. Velocities, accordingly, are determined relative to the reference velocity so that directional ambiguity is avoided.

12

Light scattered from particles passing through the probe volume is received by a photomultiplier tube (PMT) through the collector optics. By viewing the probe volume through an aperature at an off-axis collection angle, one can vary the effective probe volume length. The collector optics were positioned so that operation was in the backscatter mode. The system had the capability to measure velocities over an axial velocity range $-250 \leqslant u \leqslant 700$ ft/sec and a vertical velocity range $-250 \leqslant v \leqslant 250$ ft/sec.

The laser velocimeter was mounted on a traverse system which allowed movement of the probe volume along any of three mutually orthogonal axes. When the flow is traversed along the vertical diameter of the duct, the vertical fringes provide the radial velocity of the flow field and the horizontal fringes provide the axial velocity component. By positioning the probe volume at a point along the vertical diameter, one could simultaneously record samples of both the axial and radial velocity components and average these to provide axial and radial velocity moments and the $\overline{u'v'}$ correlation at each sampled point.

In some flows natural seeding may be adequate for acquiring laser velocimeter measurements. However, at the temperatures in the chemically reacting flow field, not enough natural particles survive to permit obtaining velocity measurements within a reasonable time period. Thus, a particle seeding device was developed (Fig. 7) with which the primary air stream was seeded. Uniform $1$-$\mu$-diam particles were used in the seeder because they should trace the fluid motion with reasonable accuracy. It is likely, however, that actual particle sizes larger than $1$ $\mu$ were encountered because of particle agglomeration.

Two operational problems were encountered in acquiring LV data through the slot in the cell wall. Water, formed in the combustion process, deposited on the quartz window surface. It was necessary to shield the viewing port area with baffles and heat the window surface during the test to avoid condensation which could attenuate the LV signal. In addition, the test apparatus moved slightly during testing because of thermal expansion, necessitating realignment of the LV with respect to the flow-field centerline at each axial position.

## 2.3 PRECISION OF MEASUREMENTS

The uncertainty of a measured parameter was determined from the bias limits and precision indices of the instrumentation by the procedures developed in Ref. 9. Given the bias limits and precision indices associated with the measurements necessary to define any parameter ($\Phi$), the total uncertainty in $\Phi$ is defined as

$$U_\Phi = \pm(B_\Phi + t_{95} S_\Phi) \qquad (2)$$

13

where

$$B_\Phi = \sqrt{\sum_{i=1}^{N} \left[ \left(\frac{\partial \Phi}{\partial \xi_i}\right) B_{\xi_i} \right]^2} \qquad (3)$$

is the bias limit for $\Phi$.

$$S_\Phi = \sqrt{\sum_{i=1}^{N} \left[ \left(\frac{\partial \Phi}{\partial \xi_i}\right) S_{\xi_i} \right]^2} \qquad (4)$$

is the precision index for $\Phi$. and $\xi$ is the measured parameters which define $\Phi$; that is,

$$\Phi = \Phi(\xi_i), \quad i = 1, \ldots, N \qquad (5)$$

and N is the number of measured parameters that define $\Phi$. The parameter $t_{95}$ is the 95 percentile point for the two-tailed student "t" distribution.
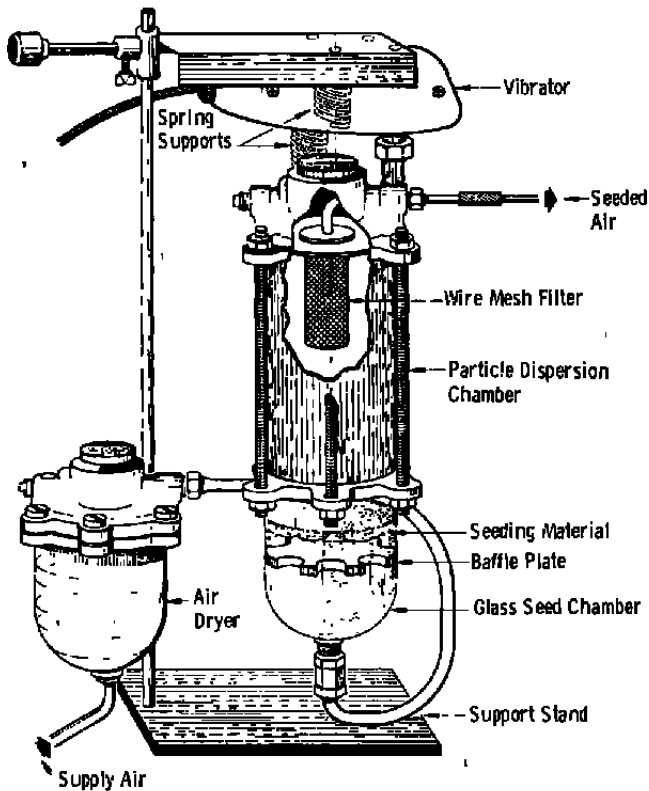


Figure 7. Fluidized bed seeder.

14

The bias limits and precision indices of instruments vary with the magnitude of measured quantities. Therefore, representative test conditions were selected upon which to base the precision indices and bias limits. Uncertainties in the fundamental measured parameters are presented in Table 1.

The instrument uncertainty of a Bragg-diffracted laser velocimeter is dependent on the accuracy to which the fringe spacing can be determined, the stability of the crystal oscillator used to drive the Bragg cell, and the precision to which the Doppler Data Processor (DDP) can determine the signal period. The uncertainty in the LV fringe spacing, $\Delta K_u/K_u$, evaluated as described in Ref. 10 from LV calibrations, is ±0.025 for the horizontal fringe spacing $K_u$ of 40$\mu$m and ±0.010 for the vertical $K_v$ of 13.4 $\mu$m. Tests of the stability of the crystal oscillators used in these experiments indicate that the uncertainty in the Bragg frequency ($\Delta f^*/f^*$) is ±6.66 x 10$^{-4}$ and ±7.69 x 10$^{-4}$ for the horizontal and vertical measurements, respectively. A detailed study of DDP accuracy showed that the processor used to measure axial velocity had an accuracy ($\Delta\tau_i$) of ±0.005 nsec, whereas the DDP used for vertical velocities was accurate within ±0.05 nsec. For these values, Ref. 8 gives the uncertainty in the axial velocity measurements as ±4 percent of the measured value at -100 ft/sec and ±3 percent at 700 ft/sec. The uncertainty in the radial velocity measurement is ±8 percent of the measured value at 10 ft/sec and ±3.5 percent at 30 ft/sec.

In using an individual realization LV, one attempts to reproduce the statistical behavior of a continuously variable velocity by a finite number of measurements. The results for the mean value of velocity or its standard deviation are, therefore, only approximations to the true value of these parameters. The degree of approximation can be evaluated in terms of statistical confidence levels (Ref. 7). It is shown in Refs. 8 and 11 that although the confidence interval for the mean velocity depends on the sample size and turbulence intensity, the confidence interval for the measured turbulence intensity depends, additionally, on the kurtosis of the velocity distribution. For a data set of 1,500 samples and a 95-percent confidence level, the confidence interval for the mean velocity in the recirculating flow field is less than 5 percent, but the confidence interval for the turbulence intensity is under 6.5 percent.

In addition to estimating the statistical confidence of the individual realization LV averages, this study considered statistical bias (as defined in Ref. 12). Although statistical bias might be expected to be high with the highly turbulent flow being measured (Ref. 13), it has been shown (Ref. 14) that bias is diminished when the fluid density fluctuates as it does in this hydrogen-air flow field. Furthermore, temporal fluctuations in the particle number density, which are known to occur with fluidized bed seeders (Ref. 15), can further diminish any statistical bias (Ref. 16). Therefore, statistical bias was expected

Table 1. Measurement Uncertainty

| Parameter | Representative Value of Parameter | Uncertainty,* Percent of Value |
|---|---|---|
| Wall Static Pressure | 0.04 psig | ±5.0 |
| Probe Pitot Pressure | 3 psig | ±2.0 |
| LV Measured Axial Velocity | 300 ft/sec | ±3.0 |
| LV Measured Axial Velocity | -100 ft/sec | ±4.0 |
| LV Measured Radial Velocity | 30 ft/sec | ±3.5 |
| LV Measured Radial Velocity | 10 ft/sec | ±8.0 |
| Hydrogen Mass Fraction (Nonreacting) | 0.03 | ±5.0 |
| Hydrogen Mass Fraction (Reacting) | 0.04 | ±16.0 |
| Primary Air Mass Flow | 0.580 lbm/sec | ±2.0 |
| Secondary Hydrogen Mass Flow | 0.002 lbm/sec | ±6.0 |
| Probe Radial Position | 3 in. | ±6.2 |
| Probe Axial Position | 30 in. | ±1.4 |
| Laser-Raman Measured Temperature | 2,000°R | ±10 |
| Laser-Raman Measured Concentration | 0.6 | ±25 |

*Uncertainty determined from technique presented in Ref. 9.

to be inconsequential in this study; however, to verify this expectation some data were randomly sampled as suggested in Ref. 17. Averages of all the randomly chosen data agreed with arithmetic averages of the original data, and this agreement indicates that no significant statistical bias exists.

## 2.4 TEST PROCEDURES

Prior to each test period the pressure and temperature instrumentation were calibrated by the application of known voltages to determine instrument response. Calibration factors for the probe-extracted concentration instrumentation were obtained from application of a set of $H_2$-$N_2$ gas mixtures of known molecular weight. The sensitivity of each measurement system was obtained over the range of values expected during the test. Data other than manometer pressures were recorded on a high-speed minicomputer data acquisition system. The impact probe pressure was also displayed on an x-y recorder.

Prior to each test the LV laser was adjusted to obtain the 514.5-nm spectral line; then the Bragg cell beam splitter was balanced to obtain equal intensities in four beams. After the adjustments were completed, the fringe spacing and orientation of the moving fringes with respect to the jet axis were determined. A detailed discussion of the procedure is presented in Ref. 10. A high-speed minicomputer data acquisition system was used to acquire the LV data.

To initiate the combustion process, a mixture of hydrogen and air in the test cell was ignited at very low flow rates. The flows were carefully increased together to avoid flame blowout. Conditions were set by establishing the desired flow rates of air and hydrogen as indicated by the pressure and temperatures upstream of the metering venturis. The LV and laser Raman (LR) data were taken during different test periods from the probe data (total pressure and gas composition) so that the probe would not perturb the flow field while the optical measurements were being made.

For probe data acquisition the nozzle assembly was positioned at a desired distance from the probe. A continuous x-y plotter trace of total pressure versus radial position was taken to guide the selection of the radial locations to record total pressure and gas composition data. The probe was then incrementally stepped across the stream to obtain pressure and gas composition profiles.

To obtain LV data, first the LV probe volume was positioned on the horizontal centerline of the test cell, and then the laser velocimeter was traversed vertically to record data at prescribed increments. Similarly, to obtain laser Raman data, the spectrometer was first positioned on the horizontal centerline of the test cell and then traversed vertically to record data at prescribed increments. It was necessary to realign both the LV and the LR with respect to the duct centerline each time the nozzle assembly was repositioned because of movement of the duct from thermal expansion caused by the change in the location of the combustion region.

## 3.0 RESULTS AND DISCUSSION

Experimental data were obtained in a ducted, subsonic, axisymmetric, recirculating flow field, both with and without chemical reactions. The primary jet airflow rate was 0.580 lbm/sec, and the secondary, outer stream, hydrogen flow rate was 0.002 lbm/sec. These flow rates result in a fuel/air ratio (F/A) of 0.00345 lb $H_2$/lb air where the stoichiometric F/A ratio is 0.025 lb $H_2$/lb air. The one-dimensional velocity of the primary and secondary streams was 335 ft/sec and 3 ft/sec, respectively, and the inlet temperatures were nominally 60 and 100°F, respectively. The fully mixed temperatures were nominally 65°F for the nonreactive case and 1,300°F for the reactive case. The nominal static pressure in the exhaust duct was 13.7 psia. Measurements were made at

17

axial stations from zero to six duct diameters from the primary nozzle exit plane. The data included radial distributions of hydrogen mass fraction, mean axial velocity, mean radial velocity, axial turbulence intensity, radial turbulence intensity, velocity cross correlation, rotational temperature, air species number density, and total pressure. In addition, the mixing duct wall static pressure distribution was obtained. The nominal test conditions are presented in Table 2, and the data are tabulated in Appendix A.

## Table 2. Nominal Test Conditions

| Parameter | Nominal Value |
|-----------|---------------|
| F/A | 0.00345 lb H2/lb air |
| $\dot{W}_p$ | 0.580 lbm/sec |
| $\dot{W}_s$ | 0.002 lbm/sec |
| $P_s$ | 13.7 psia |
| $T_{Tp}$ | 520°R |
| $T_{Ts}$ | 560°R |
| $u_p$ | 335 ft/sec |
| $u_s$ | 3 ft/sec |

## 3.1 PRESSURE MEASUREMENTS

The axial distribution of wall static pressure is shown in Fig. 8. The nonreactive pressure distribution is typical of distributions encountered in separated, reattached flows. However, the static pressure rise for the reactive recirculating flow is seen to be significantly different from the nonreactive case. The pressure distributions clearly indicate that one significant effect that the chemical heat release has on the recirculating flow field is to change the rate of wall static pressure rise.

The radial distributions of total pressure are shown in Figs. 9 and 10. A comparison of the data in the two figures reveals that the total pressure decay is slowed by the chemical heat addition, indicating that the effect of the chemical reaction is to reduce the momentum transport rate of the two coaxial streams. The shape of the total pressure profiles also demonstrates the reduced mixing rate. For the nonreactive case, the total pressure profile is essentially flat at X/D = 5, but for the reactive case a significantly nonuniform profile still exists at X/D = 6.

18
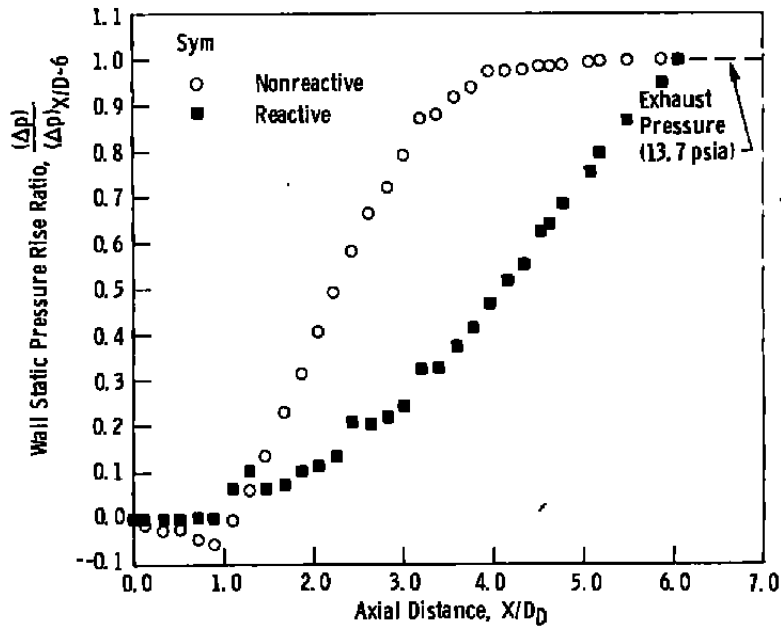
Figure 8. Axial distribution of wall static pressure.
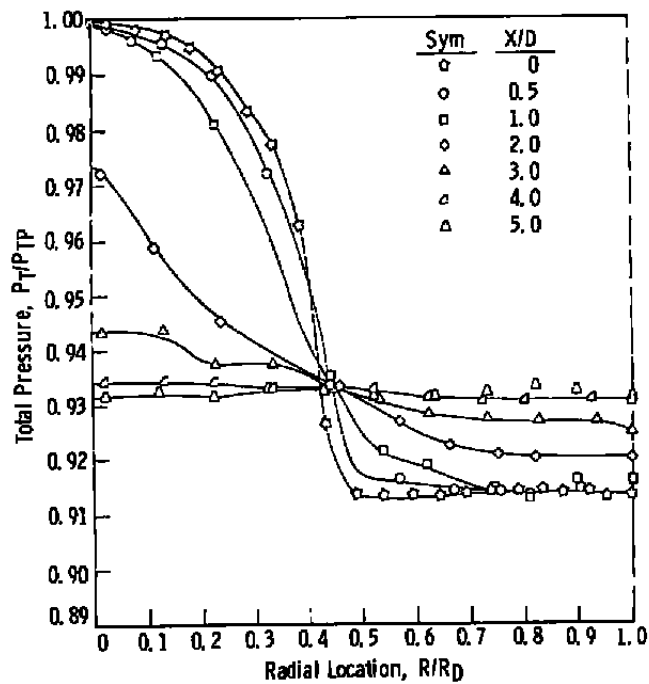


Figure 9. Radial distribution of total pressure without chemical reactions.
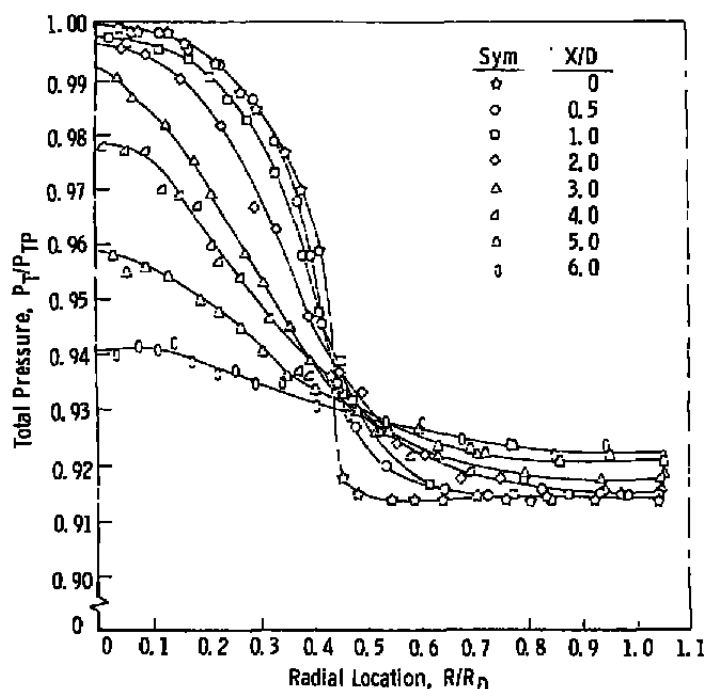
**Figure 10. Radial distribution of total pressure with chemical reaction.**

## 3.2 LASER VELOCIMETER MEASUREMENTS

Representative radial distributions of mean axial velocity, mean radial velocity, axial turbulence intensity, radial turbulence intensity, and the velocity cross correlation are shown in Figs. 11 through 15 both with and without chemical reaction. The velocity data are nondimensionalized by the one-dimensional primary jet flow velocity, $u_p$, and the axial and radial distances are ratioed to the duct diameter and radius, respectively. Data are presented for three representative axial locations for the purpose of clarity. The complete data package for all axial locations is tabulated in Appendix A.

It should be noted that only the center jet flow was seeded with alumina particles. Since the outer jet bulk velocity was low, it was thought that if only the center jet were seeded, the recirculation eddy would act to distribute the seed material throughout the flow and provide a nearly uniform particle number density. For the case of flow without chemical reaction, the particle number density in the outer stream was sufficient to provide an acceptable data rate, and thus valid velocity measurements were obtained across the entire duct. However, for the case of flow with chemical reaction, the alumina deposited on the walls, and as a result the recirculation eddy did not distribute sufficient seeding material across the outer stream in the region near the primary nozzle exit plane.

Therefore, velocity measurements could not be obtained in the flow near the duct wall in a reasonable sampling time.

The data presented in Figs. 11 through 15 show radial profiles of velocities at representative axial locations both with and without chemical reactions to demonstrate the effect of the chemical heat release on the parameter. It is evident from the mean axial velocity variation (Fig. 11) that chemical heat addition broadens the radial profile and reduces the axial velocity decay. The profiles of radial velocity (Fig. 12) also indicate, although less dramatically, the sustained high velocity resulting from the chemical reaction. The maximum value of the turbulence intensity, $u'/u_p$ and $v'/u_p$ (Figs. 13 and 14), is about the same for the two cases. However, the axial location of the maximum turbulence intensity (not shown) is reached closer to the primary nozzle exit plane in the nonreacting case because in each case the location of the maximum turbulence intensity occurs near the center of the mixing zone, which extends farther downstream with chemical reaction. The turbulence intensity becomes essentially constant by $X/D = 4$ for the nonreactive case, whereas significant nonuniformity still exists at $X/D = 6$ for the reactive case. Note by comparing the data in Figs. 12 and 14 that the magnitude of the radial turbulence intensity is much greater than the mean radial velocity at nearly every point in the flow field. The velocity cross correlation, $\overline{u'v'}/u_p^2$, shown in Fig. 15, also indicates a considerable effect of chemical heat release on
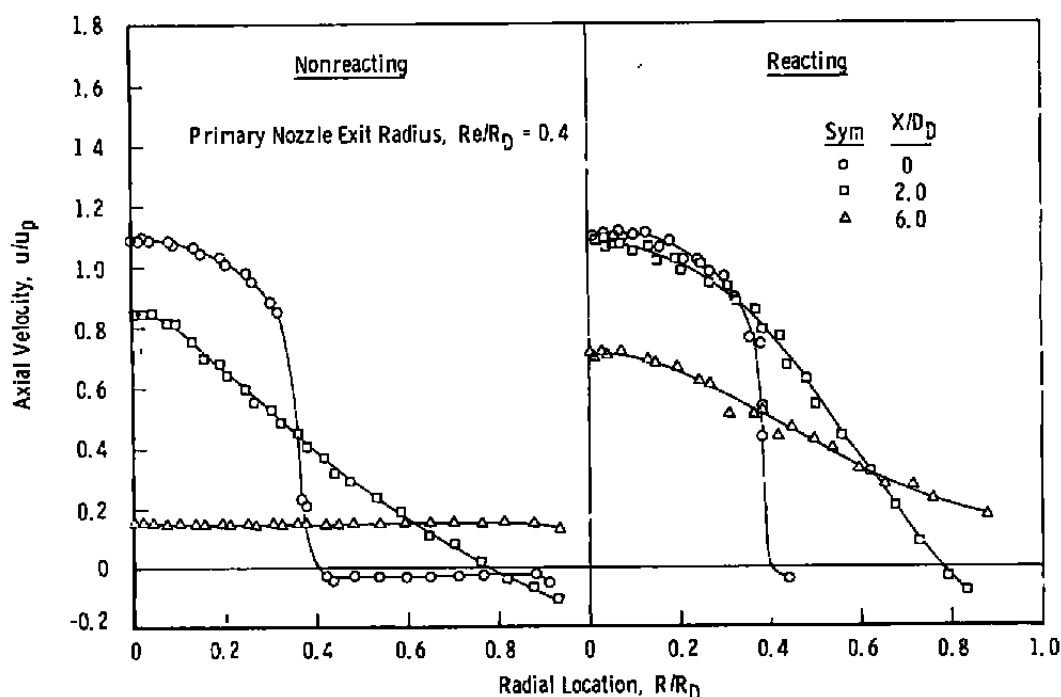


Figure 11. Radial distribution of mean axial velocity.
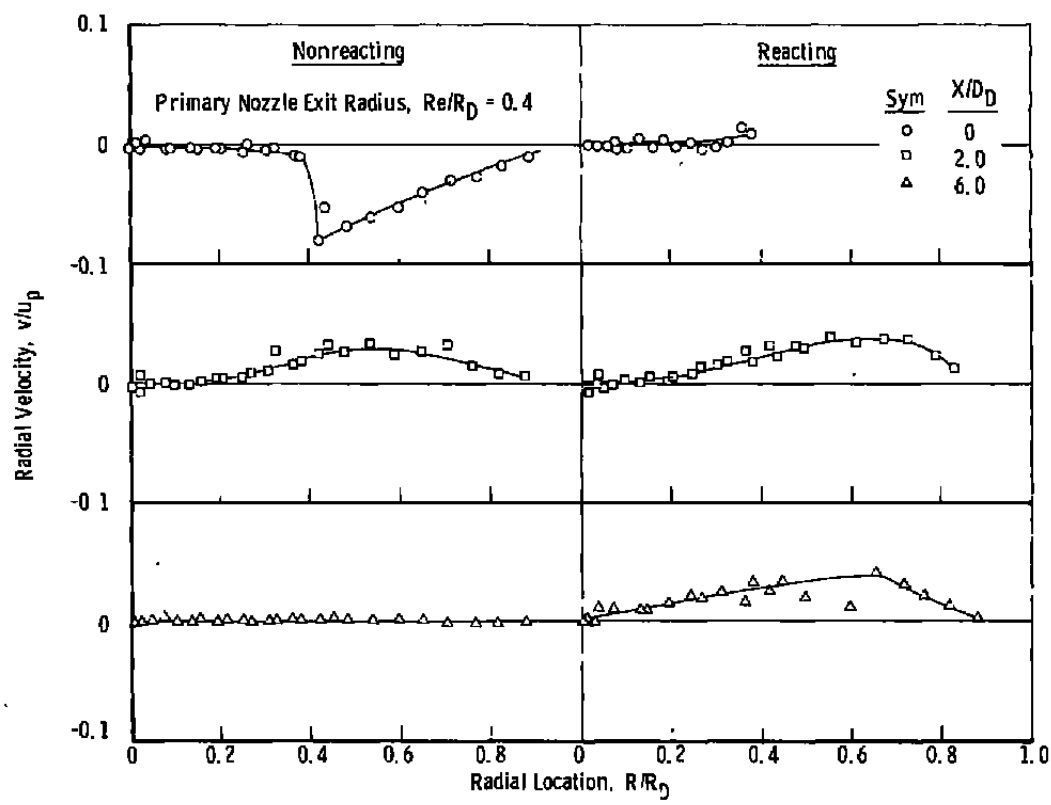
Figure 12. Radial distribution of mean radial velocity.
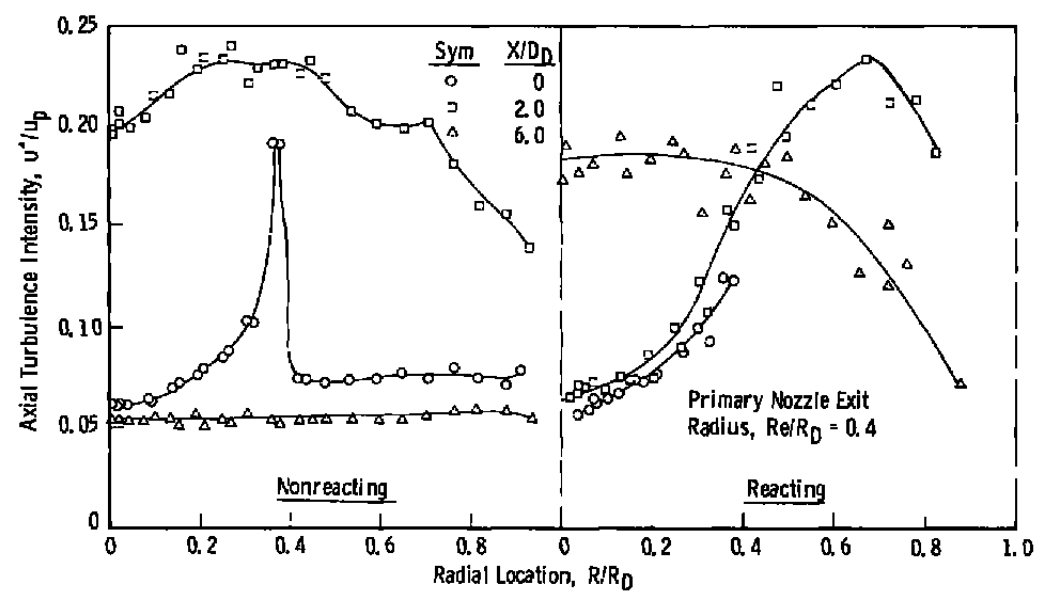


Figure 13. Radial distribution of axial turbulence intensity.
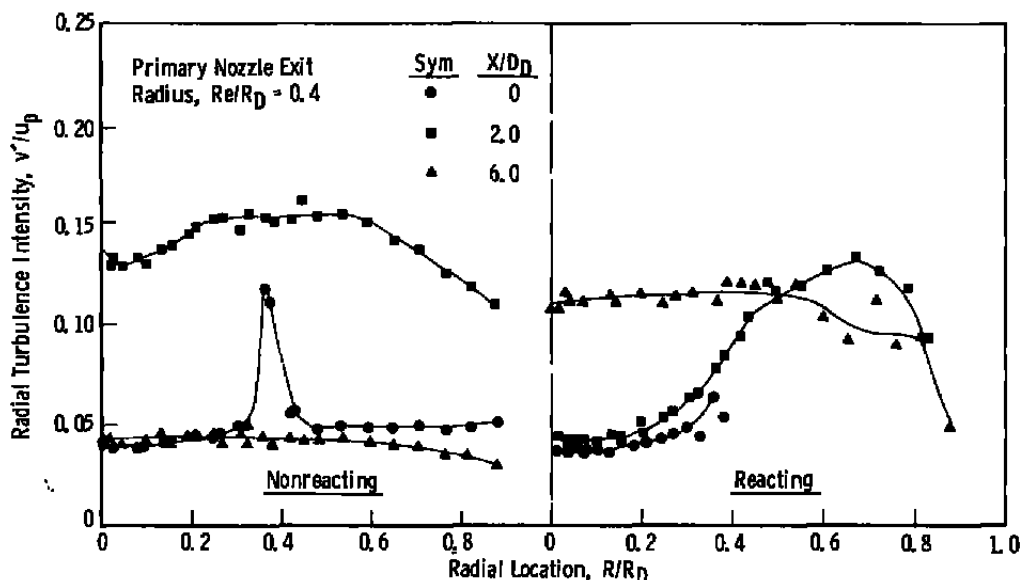
Figure 14. Radial distribution of radial turbulence intensity.

the Reynolds stress field. The decay of the mean axial velocity along the duct centerline is shown in Fig. 16. As implied from the previously presented data, the measurements reveal that the velocity decays less rapidly in the reactive case than in the nonreactive case. It has been noted in Ref. 18 that the velocity in reactive streams decays less rapidly than that in comparable nonreactive streams, but a complete explanation for this phenomenon has not been given.

Figure 17 shows the location of the locus of points of zero mean axial velocity in the recirculating flow field, both reactive and nonreactive. Note that the locus does not represent the dividing streamline and in fact corresponds to the dividing streamline at only two points, the forward and rear duct wall stagnation points (Fig. 1). A comparison of the data clearly demonstrates the effect of the chemical heat release on the location and extent of the recirculation zone. The downstream reattachment point is seen to lie between X/D = 3 and X/D = 4 for the nonreactive case and at approximately X/D = 6 for the reactive case. The result is significantly different from the results shown in Fig. 18, obtained by Schulz (Ref. 1) and Chriss (Ref. 2) on a configuration geometrically similar but with a ratio of mixing duct to primary jet diameter of 10 as opposed to the current diameter ratio of 2.5. The results of Schulz and Chriss indicate that the behavior in the location of the reattachment point and the shape of the zero velocity locus curve are essentially identical for the reactive and nonreactive cases. However, the diameter ratio 10 configuration is about the upper limit for aerospace applications. The diameter ratio 2.5 configuration is more typical of a ramjet dump combustor.

23
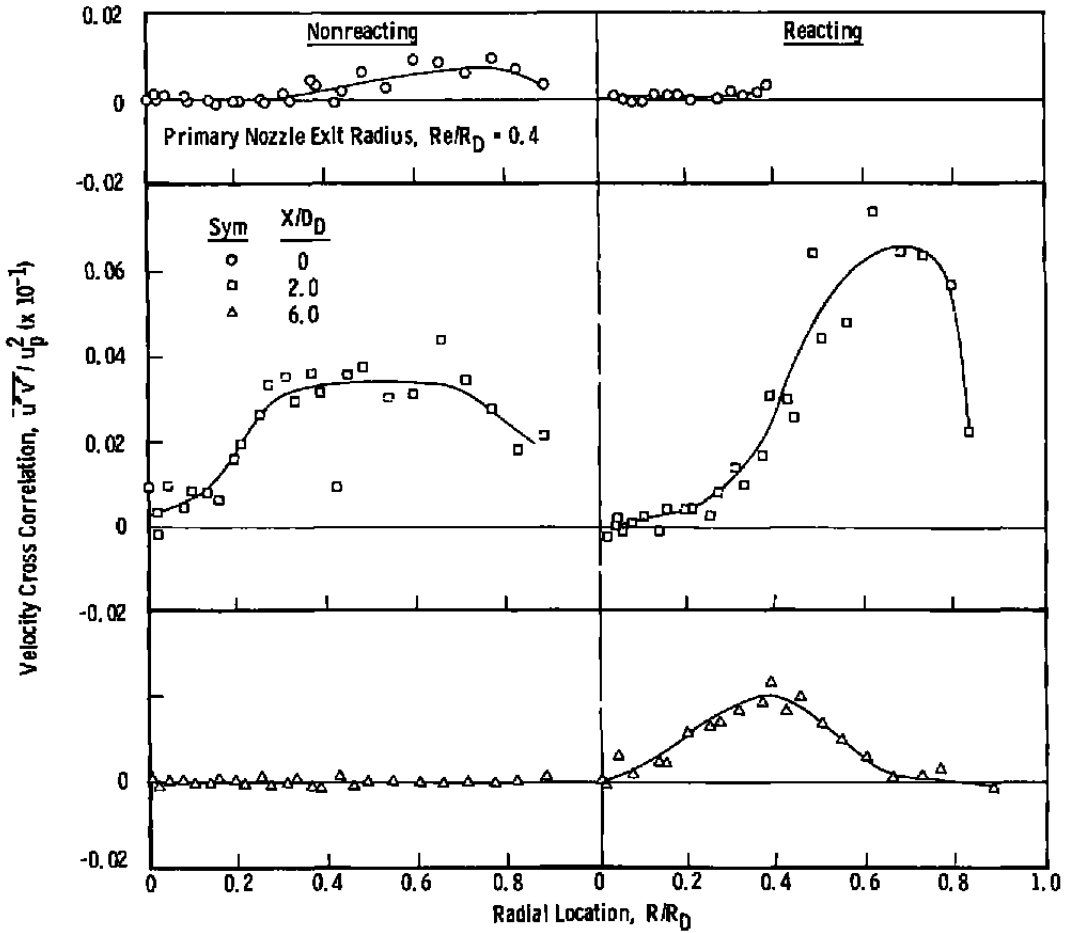
Figure 15. Radial distribution of the velocity cross correlation.

## 3.3 HYDROGEN MASS FRACTION

For the chemically reacting hydrogen-air mixture, the elemental hydrogen mass fraction ($F_H$) is related to the mixture molecular weight (W) through the following general chemical relationship:

$$\beta_H \, F_H \, H_2 + \beta_O (1 - F_H)O_2 + \beta_N (1 - F_H)N2 - \beta_A (1 - F_H)A \longrightarrow$$
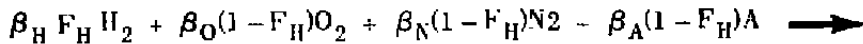
$$\beta_H \, F_H \, H_2O + \left[ \beta_O (1 - F_H) - \frac{\beta_H \, F_H}{2} \right] O_2 + \beta_N (1 - F_H)N_2 - \beta_A (1 - F_H)A \qquad (6)$$

By substituting the appropriate molecular weights, one obtains

24

$$F_{11} = \frac{2.167}{W} - 0.07481 \tag{7}$$

The mixture molecular weight, W, was obtained from the thermal conductivity analysis cell as a direct function of detector millivolt output by calibrating the apparatus using various mixtures of hydrogen/nitrogen of known molecular weights.

The radial distributions of $F_H$ for the nonreactive case are shown in Fig. 19. As expected, because of the mixing process, the centerline value of $F_H$ increases and the near-wall value decreases with increasing axial distance from the primary nozzle exit plane. Note that no pure hydrogen was measured even close to the primary nozzle exit plane. This should be expected since the velocity data indicate that the recirculation zone extends all the way back to the nozzle exit plane. In addition, the low values of $F_H$ and the highly turbulent velocity field near the wall indicate that counterstream turbulent diffusion of species apparently causes dilution of the hydrogen stream. This result is consistent with the results of Chriss (Ref. 2) for the diameter ratio 10 configuration.

For the reactive case, the probe-extracted samples were analyzed in an infrared emission-absorption cell apparatus from which the water vapor partial pressure (hence mole fraction) was directly obtained from Beer's Law (Ref. 5). The chemical balance of Eq. (6) demonstrates that the hydrogen mass fraction is directly related to the water
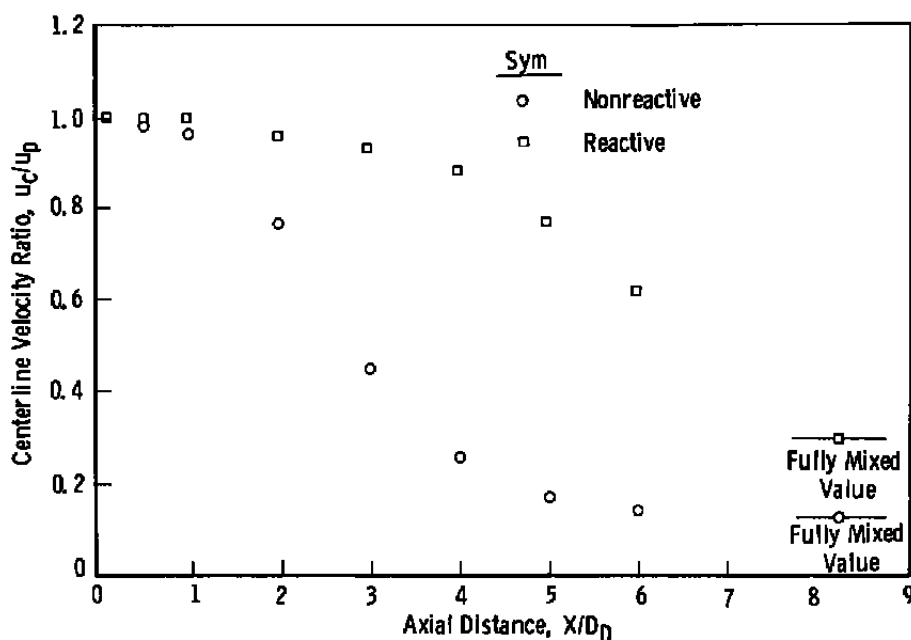


Figure 16. Axial distribution of centerline velocity.

25
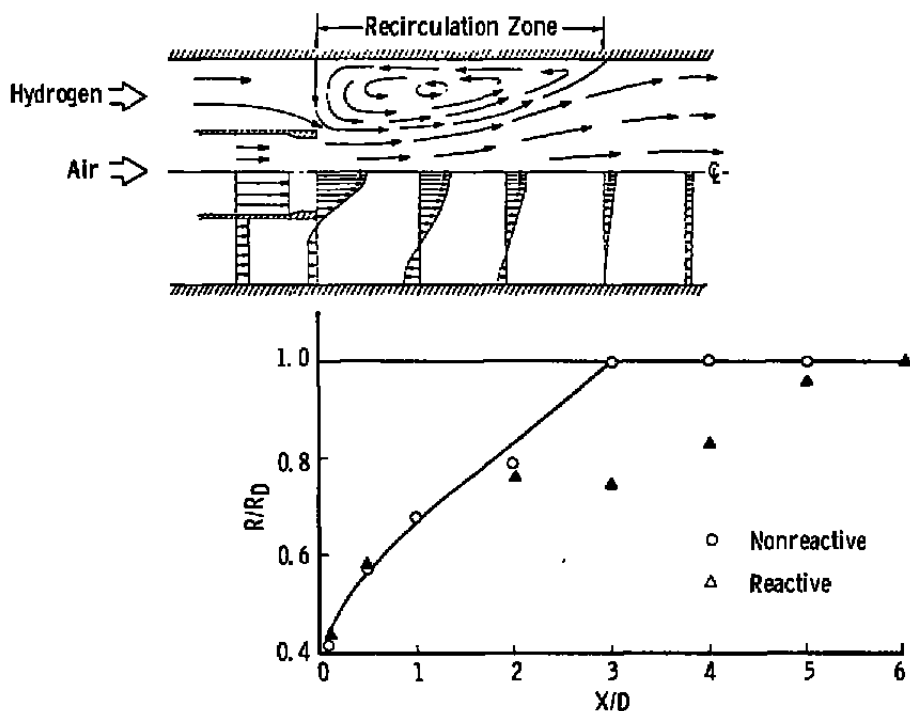
Figure 17. Locus of zero mean axial velocity points (diameter ratio 2.5 configuration).

| Sym | F/A | Configuration |
|-----|------|-----------------------|
| □ | 0. 143 | Reactive (Ref. 2) |
| ○ | 0. 107 | Reactive (Ref. 2) |
| —— | 0. 14 | Nonreactive (Ref. 1) |
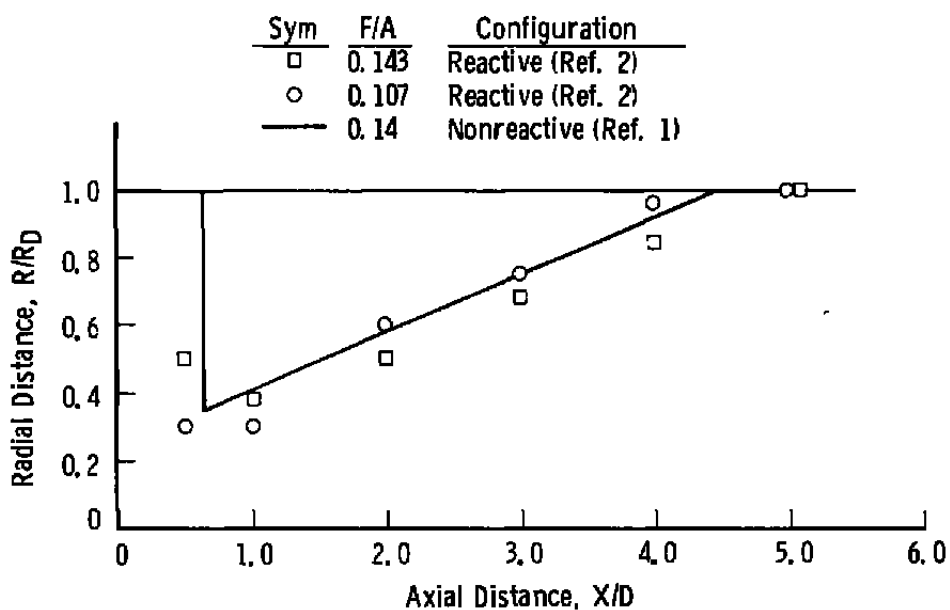


Figure 18. Locus of zero mean axial velocity points (diameter ratio 10 configuration) (Ref. 2).

vapor mole fraction. The radial distributions of $F_H$ increase and the wall value decreases with increasing axial distance from the primary nozzle exit plane. As before, no pure hydrogen was measured in the flow field, again indicating that counterstream turbulent diffusion of species apparently causes a dilution of the hydrogen stream. However, the data indicate that the mixing is less rapid in the reactive than in the nonreactive case, causing the dilution of the hydrogen stream to be less rapid.
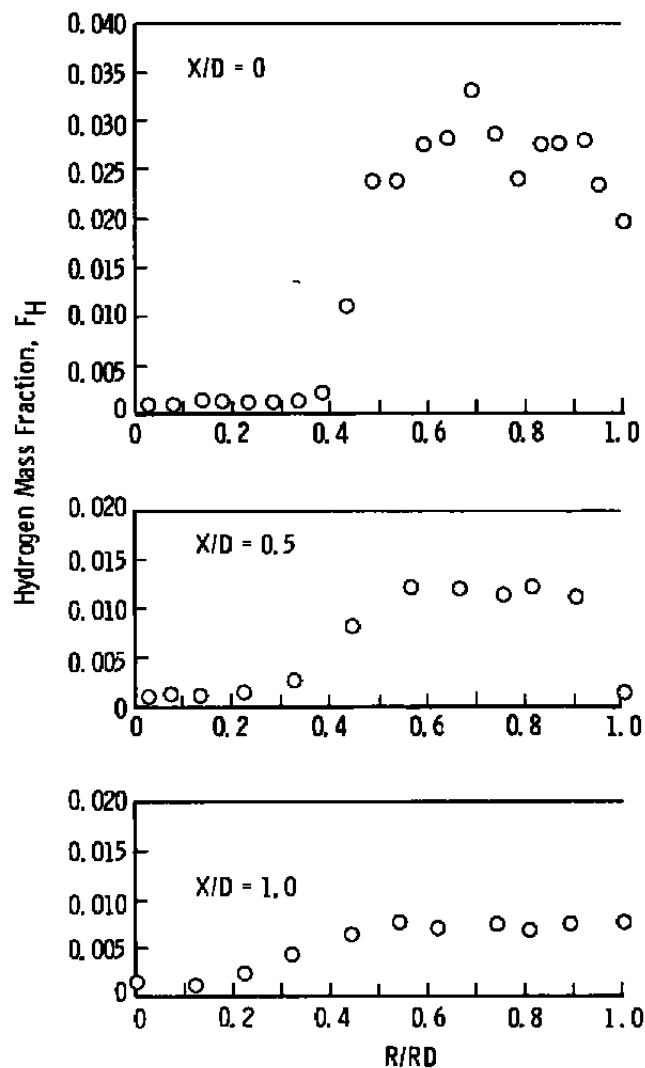


Figure 19.  Radial distributions of hydrogen mass fraction (nonreactive).
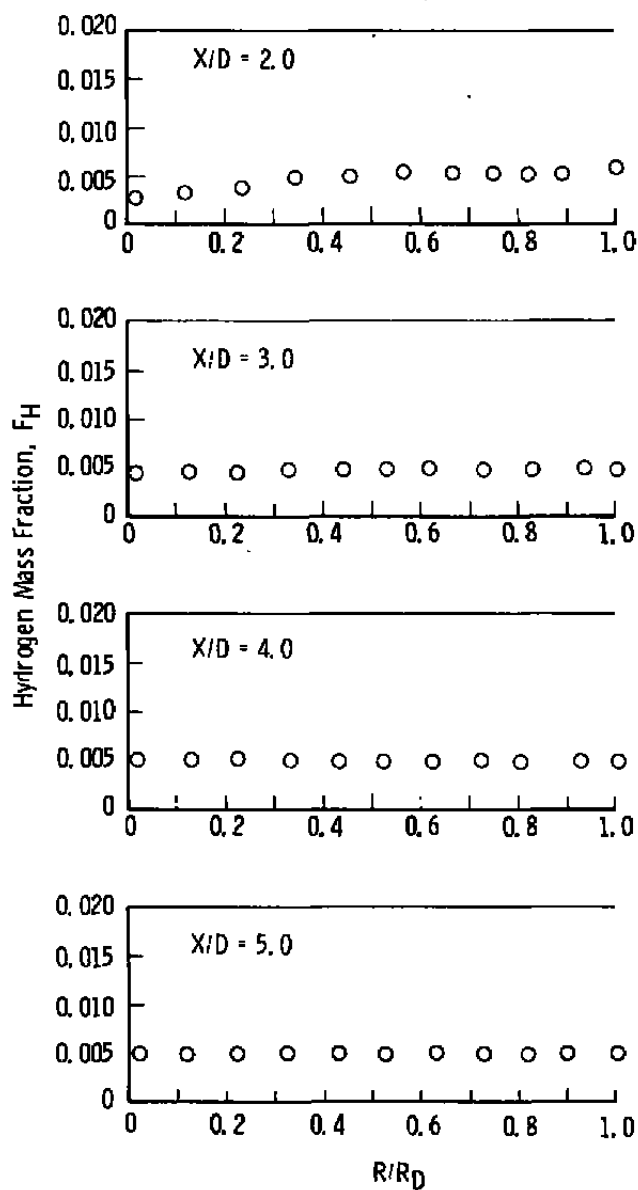
Figure 19. Concluded.
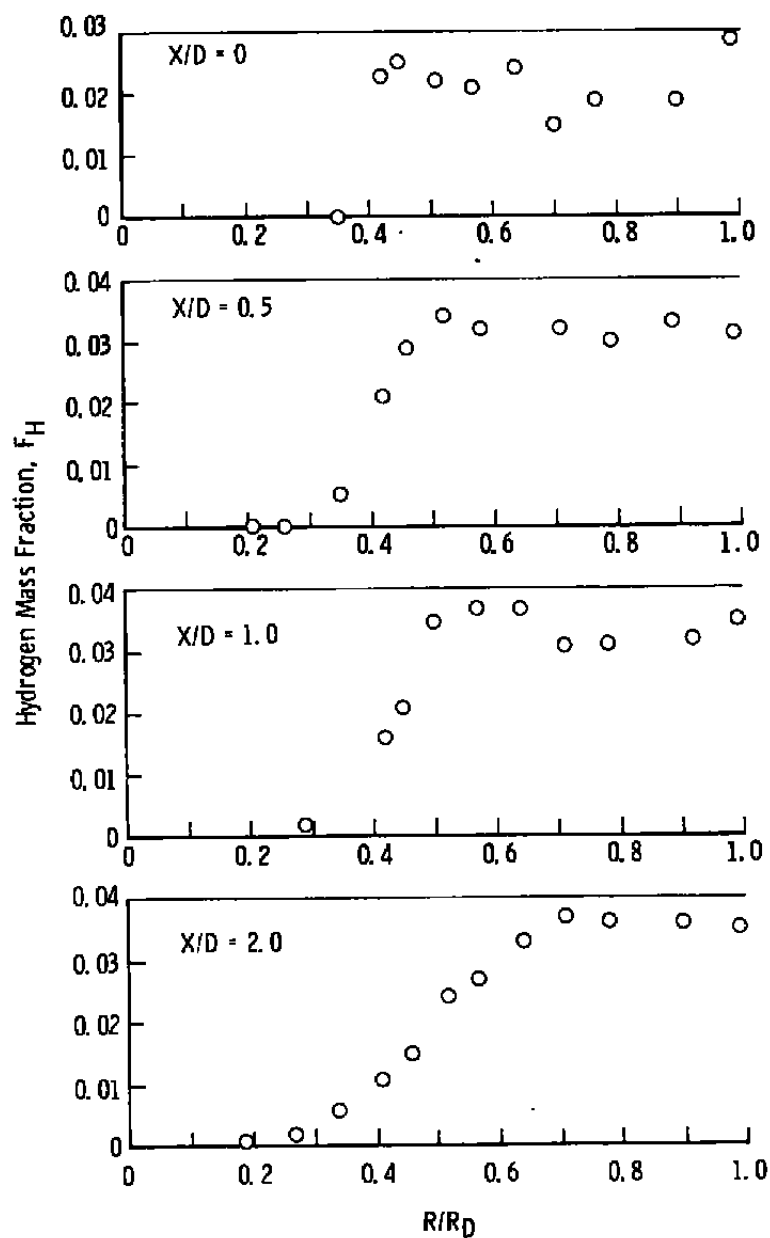
Figure 20. Radial distributions of hydrogen mass
fraction (reactive).
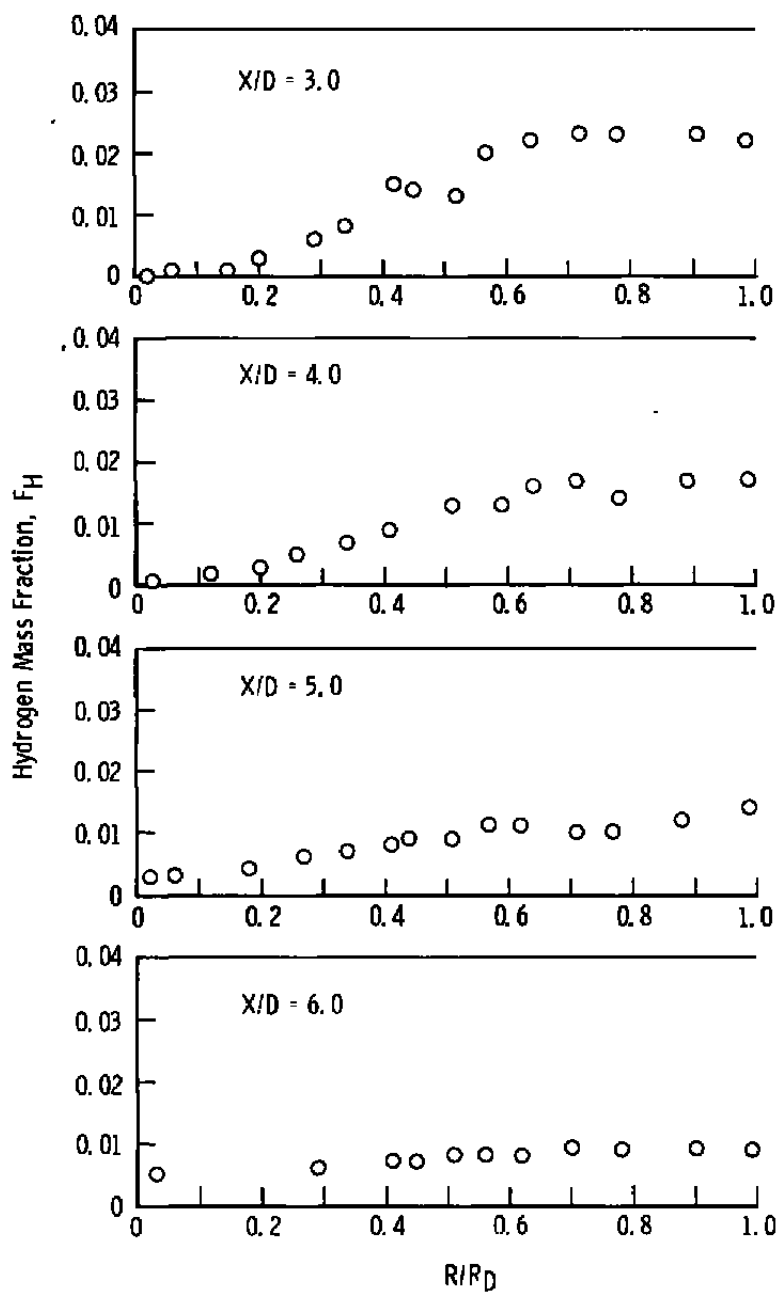
Figure 20. Concluded.

The axial distribution of $F_H$ along the mixing duct wall is presented in Fig. 21 for both reactive and nonreactive cases. The data show that at the nozzle exit plane, $F_H$ is higher for the reactive case than for the nonreactive case. The nonreactive $F_H$ decays more rapidly than the reactive, indicating more rapid mixing in the nonreactive flow field, which is consistent with the previously presented pressure and velocity data. The data also indicate that the upstream diffusion of species extends to the primary nozzle exit plane since $F_H$ is less than unity in this region. This result is consistent with the results of Chriss (Ref. 2) for the diameter ratio 10 configuration. The data also indicate that the nonreactive $F_H$ decays to the fully mixed value by $X/D = 6$ while for the reactive data mixing is not complete at this station.
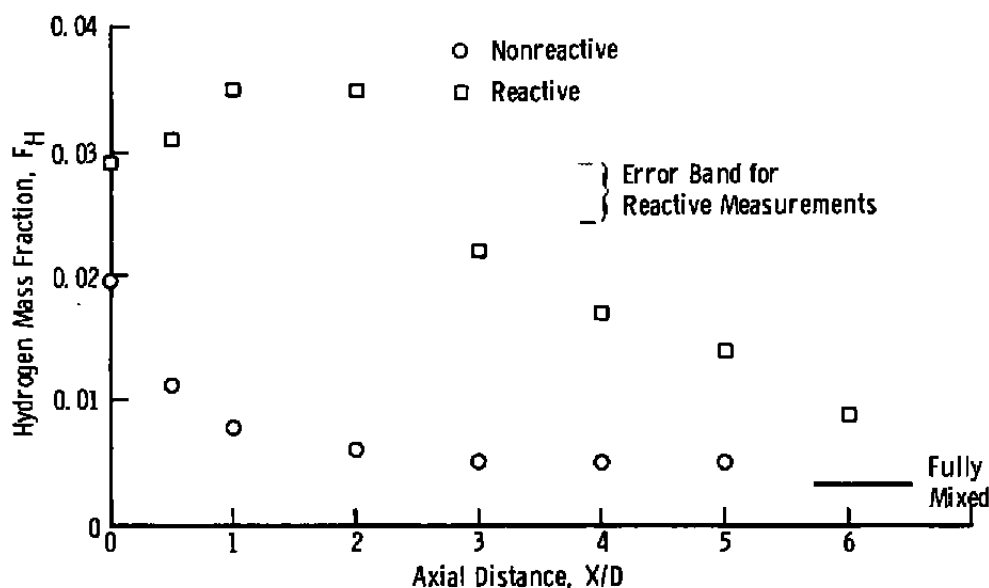


Figure 21. Axial decay of hydrogen mass fraction at $R/R_D = 1.0$.

## 3.4 LASER-RAMAN MEASUREMENTS

Radial distributions of mean static temperature are presented in Fig. 22 for seven axial locations in the recirculating, reacting flow field. The mean temperatures were obtained by calculating a value of temperature for each of the 15 samples measured per data point, and then arithmetically averaging the 15 temperatures to obtain a "mean" value. Eckbreth (Ref. 19) has presented an "ensemble" averaging technique for reducing laser Raman data obtained in fluctuating flow fields that yields a more realistic "mean" value of a measured quantity. The data obtained in the current flow configuration will be reduced using the Eckbreth technique, but the final data were not available for this report. Therefore, the temperature data presented in Fig. 22 should be considered to be
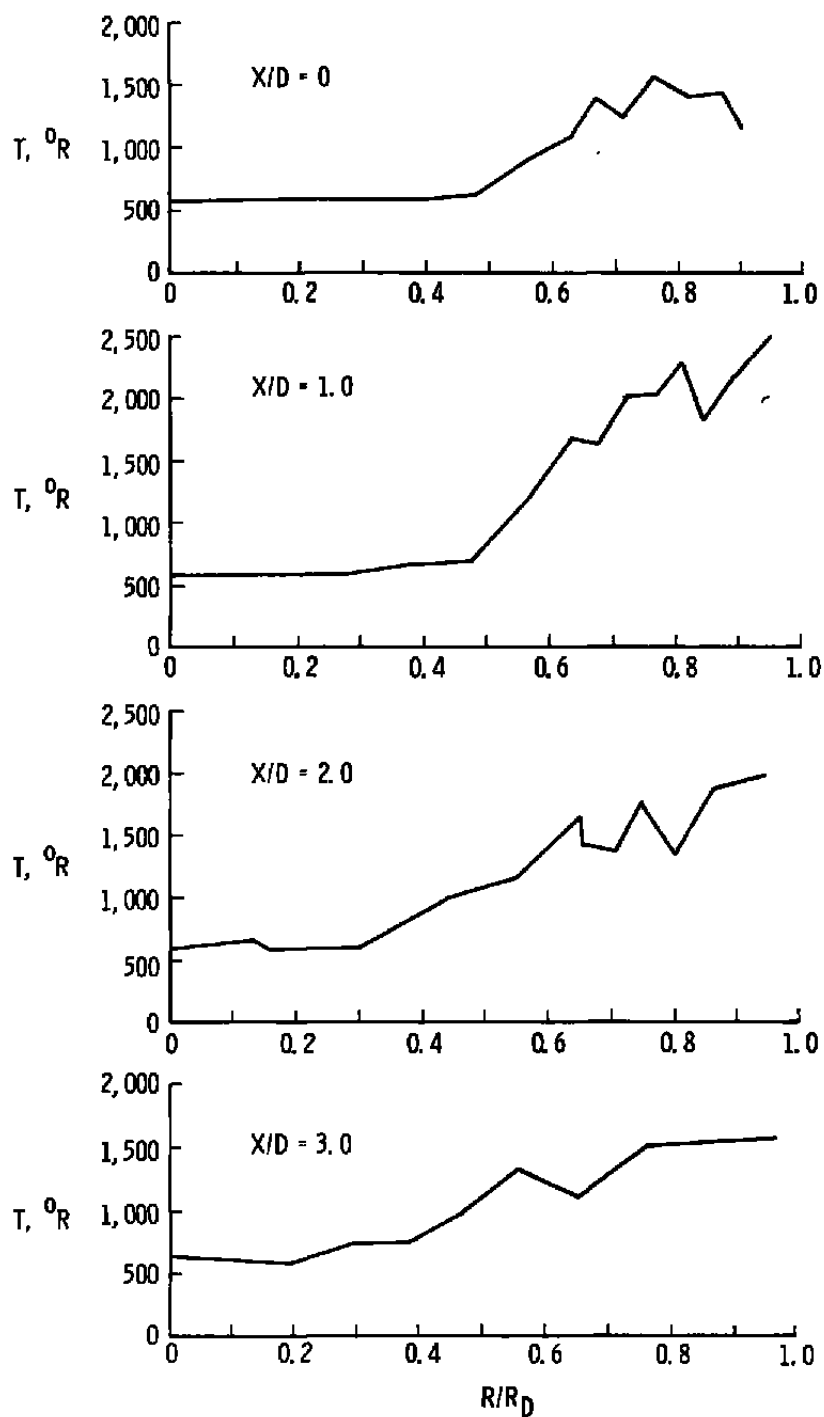
Figure 22.  Radial profiles of Raman-measured static temperature.
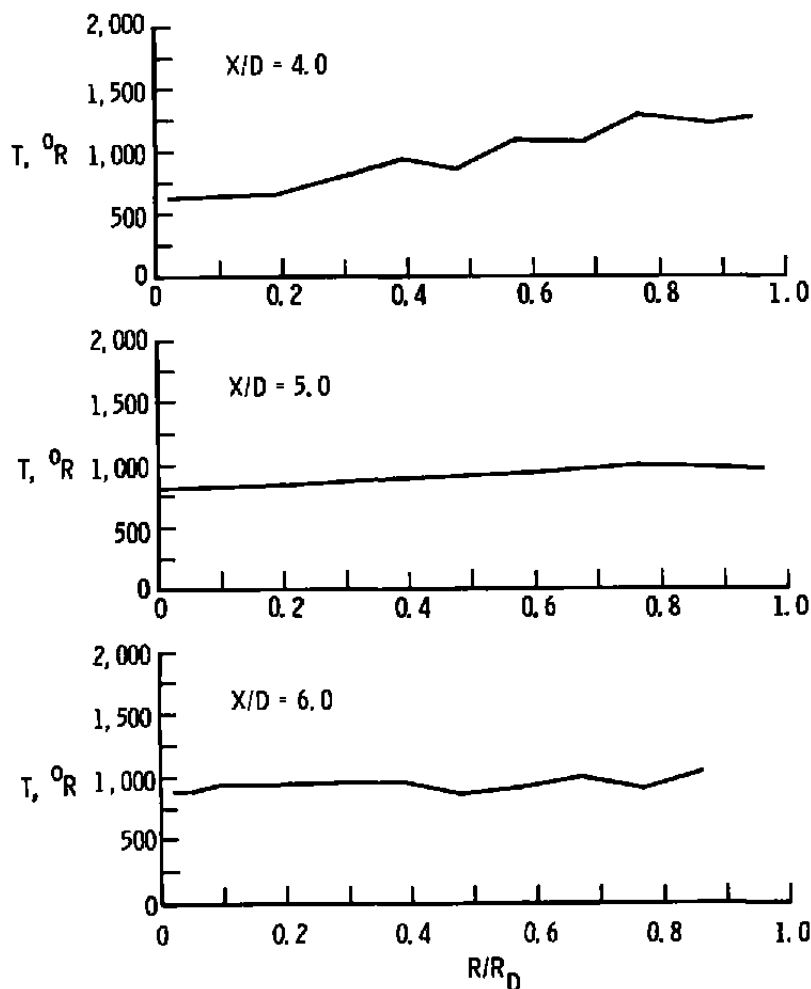
Figure 22. Concluded.

preliminary with respect to absolute value although the future planned data reduction is not expected to alter the trends shown in Fig. 22.

Similarly, the final reduction of the air specie number density data requires extensive iteration to remove the time-dependent fluctuations and produce mean values of concentration. Therefore, the air specie number densities measured during the current test program are not presented.

The radial static temperature profile data presented in Fig. 22 are tabulated in Appendix A. The temperature distributions are reasonable and as expected in that the centerline temperature is low in the near field and increases with radial distance toward the duct wall to some peak value in the turbulent recirculation zone. The radial

temperature distribution in the far field (X/D = 6) is relatively flat at a level consistent with the fully mixed fuel/air ratio when the heat loss to the water-cooled duct wall is considered. Mean temperatures at the level of stoichiometric hydrogen-air combustion (4,000°R) were not measured anywhere in the flow field, although some samples show instantaneous temperatures in excess of 4,000°R. Examination of a typical set of fifteen samples shows the instantaneous temperature values range between 1,250 and 4,100°R with a mean value of 2,540°R.

A complete explanation for the lower than expected peak temperatures is not clear at the present time although further analysis of the fluctuating instantaneous temperature data may yield some insight. The possibility exists that the relatively small number of samples obtained per data point combined with the overly simplified averaging technique may tend to obscure the existence of stoichiometric temperature values existing in the flow at least on an instantaneous basis. In addition, the spatial resolution of the laser Raman system combined with the incremental step size across the flow could result in missing locations where higher temperatures would occur, or could result in averaging temperatures over a large enough volume that the peak temperatures are obscured. Additional data reduction and analysis will continue, and the final results will be published in the near future. However, it is very clear that for future applications of a laser Raman spectroscopy apparatus to a highly turbulent recirculating combustor flow, sufficient test time must be allotted to permit on the order of 150 pulses per data point to provide data of higher statistical confidence level.

## 3.5 VELOCITY CALCULATIONS: COMPARISON WITH MEASUREMENTS

The velocities measured with the laser velocimeter are compared in Fig. 23 with the velocities calculated from the measured gas composition and pressure assuming either equilibrium chemistry with 100-percent reaction efficiency or no reactions (frozen chemistry). The two assumptions about the state of the chemistry along with an assumption of adiabatic flow allowed upper and lower limits for the velocities in the flow field to be approximated. The static pressure measured on the duct wall at the axial location of a velocity measurement was used in the calculation along with the enthalpies of the inlet systems. The calculation procedure is described in Ref. 20 and is outlined in Appendix B. The LV velocity data are seen generally to agree with the calculated velocities in level and radial profile shape. In some regions of the flow, the LV-measured velocities fall outside the limits of the two calculated velocities. This discrepancy is most probably caused by a combination of uncertainties in the measured parameters used to calculate the velocities. The discrepancy near the duct wall results from inaccurate measurements of small pressure differences (0.04 to 0.06 psia) and the inability of

34
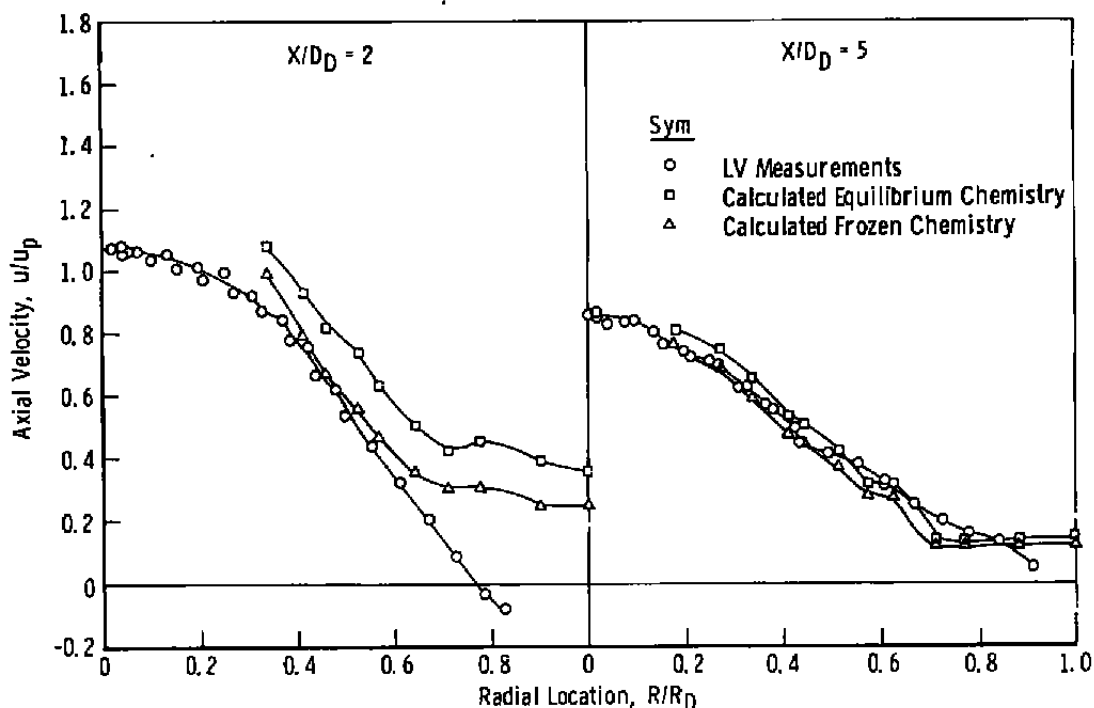
Figure 23. Comparison between measured and calculated velocities
for frozen and equilibrium chemistry.

pressure measurements to indicate flow reversals. The discrepancy near the centerline results from uncertainty in the measured hydrogen mass fraction. In general, considering all of the data, the measured velocities approach the values calculated from the equilibrium assumption at locations where complete chemical reactions would be expected and with values calculated from the frozen assumption where complete reactions would not be expected, thus indicating that the measured quantities are generally self-consistent. It must be emphasized that the calculation technique yields only approximate values of velocity within the limits of the assumptions presented in Appendix B.

## 4.0 CONCLUSIONS

Ducted, subsonic, axisymmetric, recirculating flow experiments were conducted in a combustor with a ratio of duct to inner nozzle diameter of 2.5, both with and without chemical reactions occurring. A primary jet of air at a mass flow rate of 0.580 lbm/sec was surrounded by an outer hydrogen stream at a mass flow rate of 0.002 lbm/sec. Analysis of the data led to the following conclusions:

1.  Comparison of the LV-measured velocity with that calculated from measured pressure and composition data (assuming either frozen or equilibrium chemistry) shows that the measured velocity, pressure, and composition data are self-consistent.

2.  The size and location of the recirculation zone are appreciably altered by the presence of chemical reactions. This is indicated by differences in locus of zero mean velocity locations in the recirculating zone and the wall static pressure distribution for the reactive and nonreactive cases. This result is very different from the result obtained in the diameter ratio 10 configuration (Ref. 2).

3.  The gases in a ducted, axisymmetric, reacting, recirculating flow mix more slowly than those in a nonreactive system of the same configuration and fuel-air ratio. The decay of concentration and velocity is less rapid, and the radial distributions of concentration and velocity approach uniform profiles less rapidly for the same duct length in the reacting case.

4.  The maximum value of the turbulence intensity based on the jet exit mean velocity, 335 ft/sec, is about the same for the reacting and nonreacting cases, approximately 0.25. However, the location of the maximum turbulence intensity is reached closer to the primary nozzle exit plane in the nonreacting case because in each case the maximum turbulence location occurs near the center of the mixing zone, which extends farther downstream with chemical reaction. The magnitude of the radial turbulence intensity is much greater than the mean radial velocity at nearly every point in the flow field.

5.  The hydrogen mass fraction, velocity, and turbulence intensity profiles indicate that counterstream turbulent diffusion is responsible for the dilution of the secondary hydrogen stream in the vicinity of the nozzle exit.

6.  Uncertainties in the laser-Raman temperature and concentration data indicate that in future applications to a flow similar to that investigated currently, a data rate on the order of 150 laser pulses per data point is required to provide data of a high statistical confidence level.

# REFERENCES

1. Schulz, R. J. "An Investigation of Ducted, Two-Stream, Variable Density, Turbulent Jet Mixing with Recirculation." AEDC-TR-76-152 (ADA034537), AFOSR-TR-76-1087, January 1977.

2. Chriss, D. E. "An Experimental Investigation of Ducted, Reactive, Turbulent Jet Mixing with Recirculation." AEDC-TR-77-56 (ADA044110), AFOSR-TR-77-0749, September 1977.

3. Rhodes, R. P. "Probing Techniques for Use in High Temperature Reacting Flows." AEDC-TR-68-44 (AD829143), March 1968.

4. Verdin, A. Gas Analysis Instrumentation. John Wiley and Sons, Inc., New York, 1973.

5. Limbaugh, C. C., Bertrand, W. T., et al. "Nozzle Exit Radiation Diagnostic Measurements of the AJ10-138A Improved Transtage Injector Program (ITIP)." AEDC-TR-79-29 (to be published).

6. Williams, W. D. et al. "Exhaust Plume Gas Dynamic and Radiation Measurements on a 500-lbf-Thrust Liquid Rocket Engine at Simulated Flight Conditions, Part II: Laser Raman/Mass Spectrometer Diagnostics." AEDC-TR-78-17 (ADB027812L), May 1978.

7. Bendat, J. S. and Piersol. A. G. Measurement and Analysis of Random Data. John Wiley and Sons, Inc., New York, 1966.

8. Barnett, D. O. and Giel, T. V., Jr. "Application of a Two-Component Bragg-Diffracted Laser Velocimeter to Turbulence Measurements of a Subsonic Jet." AEDC-TR-76-36 (ADA025355), May 1976.

9. Abernethy, R. B. et al., Pratt and Whitney Aircraft, and Thompson, J. W. "Handbook: Uncertainty in Gas Turbine Measurements." AEDC-TR-73-5 (AD755356), February 1973.

10. Barnett, D. O. and Giel, T. V., Jr. "Laser Velocimeter Measurements in Moderately Heated Jet Flows." AEDC-TR-76-156 (ADA038283), April 1977.

11. Cline, V. A. and Bentley, H. T. III. "Application of a Dual-Beam Laser Velocimeter to Turbulent Flow Measurements." AEDC-TR-74-56 (AD785352), September 1974.

12. McLaughlin, D. K. and Tiederman, W. G. "Biasing Correction for Individual Realization of Laser Aneomometer Measurements in Turbulent Flows." The Physics of Fluids, Vol. 16, No. 12, December 1973.

13. Barnett, D. O. and Bentley, H. T. III. "Statistical Bias of Individual Realization Laser Velocimeters." Proceedings of the Second International Workshop on Laser Velocimetry, Vol. I, ed. H. D. Thompson and W. H. Stevenson. Engineering Experiment Station, Bulletin No. 144, Purdue University, West Lafayette, Indiana, March 1974, pp. 428-444.

14. Meadows, M. D., Whiffen, M. C., and Mayo. W. T., Jr. "Laser Velocimeter for Supersonic Jet Turbulence and Turbulence Spectra Research." AFAPL-TR-74-24, Appendix IV, pp. 163-189 (1974).

15. Glass, M. and Kennedy, I. M. "An Improved Seeding Method for High Temperature Laser Doppler Velocimetry." Combustion and Flame, Vol. 29, pp. 333-335 (1977).

16. Giel, T. V., Jr. and Barnett. D. O. "Analytical and Experimental Study of Statistical Bias in Laser Velocimetry." Laser Velocimetry and Particle Sizing, ed. H. Doyle Thompson and Warren H. Stevenson. Hemisphere Publishing Corporation, New York, 1978.

17. Durao, D. F. G. and Whitelaw, J. H. "The Influence of Sampling Procedures on Velocity Bias in Turbulent Flows." The Accuracy of Flow Measurements by Laser Doppler Methods. Proceedings of the LDA-Symposium Copenhagen, Technical University of Denmark, August 1975.

18. Rhodes, R. P., Harsha, P. T., and Peters, C. E. "Turbulent Kinetic Energy Analyses of Hydrogen-Air Diffusion Flames." Acta Astronautica, Vol. I, 1970, pp. 443-470.

19. Eckbreth, A. C. "Averaging Considerations for Pulsed, Laser Raman Signals from Turbulent Combustion Media." Combustion and Flame, Vol. 31, pp. 231-237 (1978).

20. Osgerby, I. T. and Rhodes, R. P. "An Efficient Numerical Method for the Calculation of Chemical Equilibrium in the H/C/O/N/A System." AEDC-TR-71-256 (AD741825), April 1972.

21. Selby, Samuel M. CRC Standard Mathematical Tables. Chemical Rubber Company, Cleveland, Ohio, 1971 (19th Edition), pp. 558-559.

# APPENDIX A
# EXPERIMENTAL DATA

Appendix A contains a tabulation of the experimental data obtained in the present study. The data include radial distributions of mean axial and radial velocity, axial and radial turbulence intensity, velocity cross-correlation, hydrogen mass fraction, total pressure, and static temperature. Data are presented for flows both with and without chemical reactions occurring. All data are for the test conditions given in Table 2.

## Table A-1. Laser Velocimeter Data: Nonreacting and Reacting

LV DATA FOR X/D = 0.10                   — REACTING —

| R/RD | U/UP | V/UP | U'/UP | V'/UP | S AXIAL | S RADIAL | K AXIAL | K RADIAL | $\overline{U'V'}/UP^2$ (x 1,000) |
|------|------|------|-------|-------|---------|----------|---------|----------|----------|
| -0.91 | -0.051 |  | 0.078 |  | -0.17 |  | 2.39 |  |  |
| -0.88 | -0.017 | -0.011 | 0.072 | 0.053 | -0.45 | 0.17 | 3.40 | 2.61 | 0.3435 |
| -0.82 | -0.027 | -0.018 | 0.075 | 0.049 | -0.33 | 0.06 | 3.02 | 2.50 | 0.7183 |
| -0.77 | -0.023 | -0.027 | 0.081 | 0.048 | -0.40 | 0.27 | 2.71 | 2.94 | 0.9727 |
| -0.71 | -0.027 | -0.030 | 0.075 | 0.051 | -0.46 | 0.16 | 2.99 | 2.94 | 0.6187 |
| -0.65 | -0.030 | -0.040 | 0.077 | 0.050 | -0.43 | 0.25 | 2.81 | 2.78 | 0.8651 |
| -0.60 | -0.029 | -0.052 | 0.075 | 0.050 | -0.43 | 0.25 | 2.71 | 3.19 | 0.9313 |
| -0.54 | -0.029 | -0.060 | 0.074 | 0.050 | -0.51 | 0.35 | 3.02 | 3.24 | 0.2643 |
| -0.48 | -0.025 | -0.067 | 0.073 | 0.048 | -0.46 | 0.29 | 2.86 | 3.35 | 0.6369 |
| -0.42 | -0.025 | -0.079 | 0.075 | 0.056 | -0.45 | 0.46 | 2.95 | 3.40 | -0.0745 |
| -0.37 | 0.232 | -0.005 | 0.191 | 0.117 | 0.58 | -0.04 | 2.67 | 2.03 | 0.4385 |
| -0.31 | 0.884 | -0.005 | 0.103 | 0.050 | -0.22 | 0.04 | 2.73 | 3.24 | 0.1384 |
| -0.25 | 0.981 | -0.006 | 0.086 | 0.045 | -0.13 | -0.14 | 2.72 | 3.10 | 0.0131 |
| -0.19 | 1.034 | -0.002 | 0.077 | 0.044 | -0.27 | -0.14 | 2.89 | 2.95 | -0.0447 |
| -0.14 | 1.068 | -0.002 | 0.070 | 0.042 | -0.12 | 0.03 | 2.92 | 3.11 | -0.0320 |
| -0.08 | 1.090 | -0.003 | 0.064 | 0.039 | -0.10 | 0.11 | 2.93 | 3.15 | 0.0544 |
| -0.02 | 1.102 | -0.001 | 0.062 | 0.039 | -0.07 | 0.06 | 2.91 | 2.96 | 0.0221 |
| -0.00 | 1.093 | -0.003 | 0.062 | 0.041 | -0.14 | 0.15 | 2.89 | 3.10 | -0.0173 |
| 0.01 | 1.092 | 0.002 | 0.062 | 0.041 | -0.18 | -0.06 | 3.08 | 2.99 | 0.1148 |
| 0.04 | 1.091 | 0.004 | 0.062 | 0.040 | -0.21 | -0.39 | 2.95 | 2.79 | 0.0704 |
| 0.09 | 1.079 | -0.003 | 0.063 | 0.040 | -0.11 | -0.19 | 2.78 | 2.80 | -0.0412 |
| 0.15 | 1.049 | -0.003 | 0.072 | 0.042 | -0.19 | -0.27 | 2.92 | 3.01 | -0.1315 |
| 0.21 | 1.009 | -0.003 | 0.081 | 0.046 | -0.25 | -0.14 | 2.75 | 3.09 | -0.0553 |
| 0.26 | 0.553 | -0.000 | 0.089 | 0.046 | -0.21 | -0.08 | 2.77 | 2.81 | -0.0765 |
| 0.32 | 0.653 | -0.003 | 0.103 | 0.050 | -0.24 | -0.06 | 2.80 | 2.88 | -0.0363 |
| 0.38 | 0.213 | -0.010 | 0.190 | 0.111 | 0.84 | 0.12 | 3.19 | 2.15 | 1.2192 |
| 0.43 | -0.045 | -0.052 | 0.074 | 0.058 | -0.26 | 0.57 | 2.80 | 3.67 | 0.1801 |

# Table A-1. Continued

LV DATA FOR X/D = 0.50      — REACTING —

| R/RD | U/UP | V/UP | U'/UP | V'/UP | S AXIAL | S RADIAL | K AXIAL | K RADIAL | $\overline{U'V'}/UP^2$ (x 1,000) |
|---|---|---|---|---|---|---|---|---|---|
| -0.94 | -0.052 | | 0.118 | | -0.16 | | 2.12 | | |
| -0.88 | -0.096 | -0.032 | 0.110 | 0.043 | 0.05 | 0.06 | 2.34 | 2.92 | 0.1771 |
| -0.83 | -0.099 | -0.038 | 0.103 | 0.045 | 0.30 | -0.01 | 2.60 | 2.92 | 0.3681 |
| -0.77 | -0.104 | -0.048 | 0.101 | 0.052 | 0.05 | 0.11 | 2.55 | 2.90 | 0.3848 |
| -0.71 | -0.076 | -0.049 | 0.105 | 0.050 | -0.03 | -0.09 | 2.45 | 2.54 | 0.3782 |
| -0.65 | -0.068 | -0.048 | 0.104 | 0.063 | 0.01 | 0.18 | 2.57 | 2.62 | 0.0703 |
| -0.60 | -0.024 | -0.043 | 0.125 | 0.080 | 0.20 | 0.30 | 2.35 | 2.48 | 1.3901 |
| -0.54 | 0.033 | -0.035 | 0.137 | 0.092 | 0.07 | 0.17 | 2.30 | 2.29 | 1.7159 |
| -0.48 | 0.131 | -0.036 | 0.153 | 0.1C7 | -0.04 | 0.13 | 2.42 | 2.10 | 0.1405 |
| -0.42 | 0.268 | -0.024 | 0.178 | 0.120 | 0.00 | 0.01 | 2.31 | 2.22 | -0.1520 |
| -0.37 | 0.439 | -0.015 | 0.205 | 0.140 | -0.11 | -0.14 | 2.28 | 2.15 | 2.3819 |
| -0.31 | 0.722 | -0.009 | 0.203 | 0.120 | -0.64 | -0.44 | 2.84 | 2.63 | 1.6411 |
| -0.27 | 0.834 | -0.005 | 0.260 | 0.080 | -1.49 | -0.70 | 4.53 | 3.53 | -0.4851 |
| -0.19 | 1.004 | -0.005 | 0.088 | 0.059 | -0.52 | -0.66 | 3.36 | 3.87 | 0.1443 |
| -0.14 | 1.040 | -0.003 | 0.071 | 0.048 | -0.17 | -0.27 | 2.68 | 3.18 | 0.0055 |
| -0.08 | 1.070 | -0.000 | 0.065 | 0.041 | -0.17 | 0.03 | 2.73 | 2.81 | -0.0792 |
| -0.02 | 1.073 | -0.000 | 0.065 | 0.040 | -0.21 | 0.09 | 2.93 | 3.44 | 0.1065 |
| -0.00 | 1.071 | 0.002 | 0.061 | 0.042 | -0.10 | -0.06 | 2.79 | 3.29 | -0.0416 |
| 0.01 | 1.073 | 0.000 | 0.062 | 0.041 | -0.29 | -0.15 | 3.10 | 2.99 | 0.0186 |
| 0.03 | 1.066 | -0.001 | 0.063 | 0.041 | -0.28 | -0.38 | 2.87 | 3.51 | 0.0662 |
| 0.09 | 1.051 | -0.005 | 0.070 | 0.042 | -0.30 | -0.22 | 2.93 | 3.00 | 0.0423 |
| 0.21 | 0.973 | -0.012 | 0.104 | 0.068 | -0.58 | -0.64 | 3.38 | 3.60 | 0.0207 |
| 0.24 | 0.928 | -0.007 | 0.267 | 0.050 | -2.08 | -0.39 | 6.25 | 2.91 | 0.2929 |
| 0.27 | 0.874 | -0.008 | 0.156 | 0.093 | -0.96 | -0.64 | 4.17 | 2.97 | 0.8131 |
| 0.32 | 0.700 | 0.004 | 0.199 | 0.113 | -0.55 | -0.44 | 2.75 | 2.78 | 1.4553 |
| 0.38 | 0.470 | 0.001 | 0.220 | 0.140 | -0.13 | -0.17 | 2.47 | 2.16 | 1.5854 |
| 0.44 | 0.266 | 0.015 | 0.196 | 0.145 | 0.09 | 0.10 | 2.48 | 2.11 | 0.7221 |

## Table A-1. Continued

I V DATA FOR X/D - 1.00         — REACTING —

| R/RD | U/UP | V/UP | U'/UP | V'/UP | S AXIAL | S RADIAL | K AXIAL | K RADIAL | $\overline{U'V'}/UP^2$ (× 1,000) |
|------|------|------|-------|-------|---------|----------|---------|----------|---------|
| -0.93 | -0.199 |        | 0.100 |       | 0.41  |       | 3.23 |      |         |
| -0.88 | -0.171 | -0.013 | 0.116 | 0.073 | 0.73  | 0.56  | 3.61 | 3.44 | 0.2636  |
| -0.82 | -0.141 | -0.017 | 0.131 | 0.083 | 0.59  | 0.24  | 2.91 | 2.49 | 1.2541  |
| -0.76 | -0.073 | -0.010 | 0.166 | 0.094 | 0.46  | 0.22  | 2.35 | 2.34 | 2.9167  |
| -0.71 | -0.024 | 0.004  | 0.178 | 0.114 | 0.30  | 0.34  | 2.32 | 2.63 | 2.2206  |
| -0.65 | 0.084  | 0.015  | 0.210 | 0.125 | 0.04  | 0.21  | 2.34 | 2.28 | 2.5910  |
| -0.59 | 0.123  | 0.014  | 0.198 | 0.132 | -0.23 | 0.11  | 2.41 | 2.22 | 3.7087  |
| -0.53 | 0.202  | 0.024  | 0.199 | 0.135 | -0.24 | 0.04  | 2.65 | 2.31 | 1.5810  |
| -0.48 | 0.280  | 0.017  | 0.191 | 0.142 | -0.13 | 0.00  | 2.77 | 2.23 | 0.9121  |
| -0.42 | 0.385  | 0.021  | 0.203 | 0.142 | 0.07  | 0.02  | 2.63 | 2.20 | 1.6317  |
| -0.36 | 0.501  | 0.006  | 0.216 | 0.150 | -0.06 | -0.08 | 2.30 | 2.19 | 2.0426  |
| -0.31 | 0.640  | -0.005 | 0.214 | 0.129 | -0.32 | -0.32 | 2.45 | 2.46 | 1.3834  |
| -0.24 | 0.807  | 0.005  | 0.190 | 0.120 | -0.68 | -0.47 | 2.97 | 3.08 | 2.2246  |
| -0.19 | 0.931  | 0.004  | 0.150 | 0.098 | -1.00 | -0.63 | 3.96 | 3.53 | 1.1153  |
| -0.13 | 0.992  | 0.001  | 0.117 | 0.074 | -1.10 | -0.51 | 4.77 | 3.45 | 0.3503  |
| -0.08 | 1.043  | -0.002 | 0.092 | 0.062 | -0.94 | -0.44 | 4.69 | 3.79 | -0.0638 |
| -0.02 | 1.058  | -0.001 | 0.074 | 0.055 | -0.42 | -0.32 | 3.44 | 3.67 | -0.0827 |
| 0.00  | 1.054  | -0.000 | 0.076 | 0.053 | -0.50 | 0.04  | 3.60 | 3.14 | -0.1009 |
| 0.02  | 1.051  | 0.002  | 0.077 | 0.057 | -0.46 | 0.00  | 3.31 | 3.50 | 0.0158  |
| 0.04  | 1.047  | 0.004  | 0.077 | 0.055 | -0.38 | 0.11  | 3.07 | 3.57 | -0.0045 |
| 0.10  | 1.013  | -0.001 | 0.098 | 0.063 | -0.84 | -0.32 | 4.17 | 3.27 | -0.2780 |
| 0.16  | 0.961  | -0.014 | 0.132 | 0.090 | -1.22 | -0.85 | 4.94 | 3.73 | 0.4286  |
| 0.21  | 0.894  | -0.009 | 0.168 | 0.103 | -0.84 | -0.56 | 3.45 | 3.01 | 0.7141  |
| 0.27  | 0.760  | -0.008 | 0.206 | 0.127 | -0.59 | -0.36 | 2.71 | 2.64 | 0.3200  |
| 0.32  | 0.582  | 0.004  | 0.240 | 0.138 | -0.29 | -0.23 | 2.34 | 2.46 | 1.9725  |
| 0.38  | 0.487  | 0.010  | 0.217 | 0.146 | -0.04 | -0.11 | 2.46 | 2.28 | 2.0781  |
| 0.44  | 0.353  | 0.012  | 0.209 | 0.144 | -0.07 | 0.03  | 2.79 | 2.24 | 2.2371  |

## Table A-1. Continued

| R/RD | U/UP | V/UP | U'/UP | V'/UP | S AXIAL | S RADIAL | K AXIAL | K RADIAL | $\overline{U'V'}/UP^2$ (× 1,000) |
|---|---|---|---|---|---|---|---|---|---|
| −0.93 | −0.105 | | 0.139 | | 0.57 | | 2.80 | | |
| −0.88 | −0.066 | 0.006 | 0.156 | 0.111 | 0.54 | 0.45 | 2.65 | 2.77 | 2.1598 |
| −0.82 | −0.040 | 0.008 | 0.161 | 0.119 | 0.40 | 0.24 | 2.40 | 2.39 | 1.8573 |
| −0.76 | 0.029 | 0.015 | 0.181 | 0.126 | 0.26 | 0.22 | 2.46 | 2.23 | 2.8029 |
| −0.71 | 0.080 | 0.033 | 0.202 | 0.138 | 0.11 | 0.14 | 2.32 | 2.23 | 3.5032 |
| −0.65 | 0.110 | 0.027 | 0.199 | 0.142 | 0.03 | 0.01 | 2.35 | 2.26 | 4.4311 |
| −0.59 | 0.188 | 0.024 | 0.202 | 0.151 | −0.12 | −0.05 | 2.43 | 2.11 | 3.1670 |
| −0.53 | 0.237 | 0.034 | 0.208 | 0.155 | −0.08 | −0.07 | 2.57 | 2.34 | 3.0781 |
| −0.48 | 0.291 | 0.026 | 0.225 | 0.153 | −0.21 | −0.11 | 2.71 | 2.31 | 3.7844 |
| −0.42 | 0.369 | 0.025 | 0.227 | 0.152 | −0.07 | −0.09 | 2.63 | 2.22 | 0.9602 |
| −0.36 | 0.449 | 0.016 | 0.231 | 0.153 | −0.11 | −0.13 | 2.65 | 2.34 | 3.6411 |
| −0.30 | 0.524 | 0.010 | 0.222 | 0.147 | −0.18 | −0.10 | 2.63 | 2.43 | 3.5611 |
| −0.25 | 0.595 | 0.005 | 0.234 | 0.152 | −0.23 | −0.14 | 2.54 | 2.54 | 0.8802 |
| −0.19 | 0.676 | 0.004 | 0.229 | 0.145 | −0.33 | −0.27 | 2.29 | 2.50 | 1.6228 |
| −0.13 | 0.749 | −0.002 | 0.216 | 0.138 | −0.54 | −0.13 | 2.60 | 2.41 | 0.8189 |
| −0.08 | 0.809 | −0.000 | 0.205 | 0.132 | −0.66 | −0.09 | 2.82 | 2.52 | 0.4533 |
| −0.02 | 0.836 | −0.008 | 0.208 | 0.133 | −0.72 | −0.06 | 2.84 | 2.66 | 0.3421 |
| 0.00 | 0.837 | −0.003 | 0.196 | 0.136 | −0.63 | −0.13 | 2.88 | 2.82 | 0.9437 |
| 0.02 | 0.842 | 0.006 | 0.201 | 0.130 | −0.75 | −0.11 | 2.94 | 2.69 | −0.1956 |
| 0.04 | 0.840 | −0.001 | 0.199 | 0.129 | −0.86 | −0.00 | 3.23 | 2.65 | 0.9736 |
| 0.10 | 0.805 | −0.001 | 0.216 | 0.129 | −0.75 | −0.17 | 3.04 | 2.57 | 0.8513 |
| 0.15 | 0.694 | 0.002 | 0.268 | 0.140 | −0.59 | −0.22 | 2.51 | 2.52 | 0.6448 |
| 0.21 | 0.637 | 0.004 | 0.235 | 0.149 | −0.32 | −0.20 | 2.58 | 2.56 | 1.9608 |
| 0.27 | 0.551 | 0.008 | 0.240 | 0.153 | −0.23 | −0.14 | 2.40 | 2.41 | 3.3750 |
| 0.32 | 0.485 | 0.027 | 0.230 | 0.154 | −0.14 | −0.14 | 2.53 | 2.32 | 2.9732 |
| 0.38 | 0.404 | 0.019 | 0.232 | 0.151 | −0.13 | −0.07 | 2.62 | 2.20 | 3.2143 |
| 0.44 | 0.318 | 0.032 | 0.233 | 0.162 | −0.13 | 0.00 | 2.52 | 2.25 | 3.6032 |

# Table A-1. Continued

LV DATA FOR X/D = 3.01  — REACTING —

| R/RD | U/UP | V/UP | U'/UP | V'/UP | S AXIAL | S RADIAL | K AXIAL | K RADIAL | $\overline{U'V'}/UP^2$ (x 1,000) |
|---|---|---|---|---|---|---|---|---|---|
| -0.95 | 0.014 | | 0.098 | | 0.24 | | 2.32 | | |
| -0.93 | 0.026 | | 0.146 | | 0.17 | | 2.49 | | |
| -0.90 | 0.012 | -0.006 | 0.143 | 0.069 | 0.35 | 0.45 | 2.31 | 2.68 | 1.1924 |
| -0.88 | 0.049 | 0.008 | 0.149 | 0.101 | 0.21 | 0.30 | 2.57 | 2.47 | 0.2383 |
| -0.86 | 0.032 | 0.002 | 0.150 | 0.084 | 0.23 | 0.42 | 2.41 | 2.48 | 1.9580 |
| -0.82 | 0.063 | 0.021 | 0.147 | 0.121 | 0.25 | 0.25 | 2.64 | 2.37 | 1.5199 |
| -0.80 | 0.067 | -0.002 | 0.151 | 0.084 | 0.23 | 0.11 | 2.37 | 2.32 | 2.3650 |
| -0.77 | 0.075 | 0.009 | 0.161 | 0.102 | 0.25 | 0.09 | 2.43 | 2.21 | 4.0634 |
| -0.76 | 0.121 | 0.015 | 0.168 | 0.121 | 0.29 | 0.19 | 2.80 | 2.26 | 0.9903 |
| -0.71 | 0.124 | 0.025 | 0.158 | 0.133 | 0.04 | 0.06 | 2.45 | 2.29 | 2.5259 |
| -0.70 | 0.118 | 0.016 | 0.170 | 0.111 | 0.07 | 0.26 | 2.38 | 2.31 | 3.4079 |
| -0.65 | 0.165 | 0.031 | 0.178 | 0.120 | 0.09 | 0.16 | 2.62 | 2.22 | 4.3591 |
| -0.65 | 0.154 | 0.026 | 0.167 | 0.137 | 0.18 | 0.13 | 2.61 | 2.26 | 2.5806 |
| -0.59 | 0.199 | 0.034 | 0.175 | 0.121 | -0.10 | -0.11 | 2.54 | 2.26 | 4.1676 |
| -0.59 | 0.194 | 0.030 | 0.171 | 0.139 | 0.07 | 0.03 | 2.82 | 2.36 | 2.2521 |
| -0.54 | 0.220 | 0.023 | 0.174 | 0.120 | -0.06 | 0.06 | 2.34 | 2.25 | 3.6437 |
| -0.53 | 0.228 | 0.030 | 0.178 | 0.143 | 0.07 | 0.01 | 2.75 | 2.25 | 1.2262 |
| -0.49 | 0.253 | 0.032 | 0.174 | 0.144 | 0.05 | -0.05 | 2.64 | 2.28 | 0.4095 |
| -0.42 | 0.306 | 0.026 | 0.207 | 0.116 | 0.07 | -0.09 | 2.55 | 2.28 | 4.1729 |
| -0.42 | 0.302 | 0.028 | 0.194 | 0.153 | 0.16 | 0.01 | 2.57 | 2.44 | 2.3130 |
| -0.36 | 0.334 | 0.021 | 0.196 | 0.151 | 0.01 | 0.00 | 2.61 | 2.23 | 2.2349 |
| -0.31 | 0.422 | 0.022 | 0.197 | 0.111 | 0.01 | -0.10 | 2.52 | 2.33 | 3.9678 |
| -0.31 | 0.376 | 0.019 | 0.195 | 0.149 | 0.03 | 0.06 | 2.60 | 2.38 | -0.0961 |

## Table A-1. Continued

LV DATA FOR X/D = 3.01                        — REACTING —

| R/RD | U/UP | V/UP | U'/UP | V'/UP | S AXIAL | S RADIAL | K AXIAL | K RADIAL | $\overline{U'V'}/UP^2$ (x 1,000) |
|---|---|---|---|---|---|---|---|---|---|
| -0.25 | 0.402 | 0.019 | 0.202 | 0.155 | 0.14 | -0.06 | 2.62 | 2.38 | 0.7020 |
| -0.19 | 0.500 | 0.024 | 0.205 | 0.128 | -0.17 | 0.01 | 2.40 | 2.28 | 4.3924 |
| -0.19 | 0.442 | 0.018 | 0.197 | 0.160 | 0.06 | 0.01 | 2.42 | 2.27 | 1.5713 |
| -0.13 | 0.459 | 0.012 | 0.192 | 0.156 | -0.01 | 0.04 | 2.45 | 2.38 | 0.9545 |
| -0.08 | 0.529 | 0.001 | 0.187 | 0.117 | -0.22 | -0.25 | 2.24 | 2.68 | 1.0845 |
| -0.08 | 0.486 | 0.001 | 0.197 | 0.153 | 0.05 | -0.03 | 2.46 | 2.40 | 0.0725 |
| -0.02 | 0.497 | 0.004 | 0.194 | 0.157 | 0.06 | -0.02 | 2.47 | 2.32 | -1.1223 |
| -0.02 | 0.551 | 0.009 | 0.200 | 0.108 | -0.25 | 0.04 | 2.42 | 2.54 | 1.1402 |
| -0.00 | 0.485 | -0.008 | 0.191 | 0.153 | 0.04 | -0.04 | 2.53 | 2.47 | -0.2604 |
| -0.00 | 0.556 | 0.004 | 0.200 | 0.111 | -0.35 | -0.19 | 2.75 | 2.49 | 1.5671 |
| 0.02 | 0.454 | -0.002 | 0.204 | 0.152 | 0.09 | 0.10 | 2.56 | 2.32 | 0.9000 |
| 0.04 | 0.472 | 0.004 | 0.198 | 0.156 | 0.09 | 0.03 | 2.49 | 2.33 | -0.7112 |
| 0.10 | 0.477 | 0.010 | 0.199 | 0.152 | 0.01 | 0.05 | 2.50 | 2.48 | -0.6123 |
| 0.14 | 0.495 | 0.006 | 0.186 | 0.106 | -0.09 | -0.00 | 2.26 | 2.16 | 2.0802 |
| 0.15 | 0.443 | 0.013 | 0.201 | 0.149 | -0.02 | 0.10 | 2.70 | 2.34 | 1.4803 |
| 0.19 | 0.473 | 0.015 | 0.193 | 0.118 | 0.08 | -0.02 | 2.41 | 2.41 | 2.1776 |
| 0.21 | 0.411 | 0.015 | 0.192 | 0.148 | 0.07 | 0.12 | 2.72 | 2.41 | 0.6568 |
| 0.26 | 0.393 | 0.032 | 0.198 | 0.146 | 0.11 | 0.03 | 2.81 | 2.33 | 0.2280 |
| 0.32 | 0.366 | 0.044 | 0.189 | 0.151 | 0.05 | 0.08 | 2.58 | 2.33 | 0.3163 |
| 0.37 | 0.348 | 0.035 | 0.186 | 0.115 | 0.07 | 0.09 | 2.41 | 2.38 | 2.6041 |
| 0.38 | 0.323 | 0.045 | 0.193 | 0.147 | 0.00 | -0.05 | 2.84 | 2.30 | 0.5236 |
| 0.44 | 0.272 | 0.050 | 0.195 | 0.143 | 0.14 | 0.04 | 2.71 | 2.16 | 2.4802 |

## Table A-1. Continued

LV DATA FOR X/D · 4.01                    — REACTING —

| R/RD | U/UP | V/UP | U'/UP | V'/UP | S AXIAL | S RADIAL | K AXIAL | K RADIAL | $\overline{U'V'}/UP^2$ (x 1,000) |
|------|------|------|-------|-------|---------|----------|---------|----------|--------------------|
| -0.95 | 0.119 |       | 0.103 |       | 0.23 |       | 3.59 |      |         |
| -0.90 | 0.124 |       | C.107 |       | 0.24 |       | 2.87 |      |         |
| -0.88 | 0.141 | 0.007 | 0.098 | 0.077 | 0.20 | 0.97 | 3.23 | 4.64 | -0.1333 |
| -0.86 | 0.134 |       | 0.100 |       | 0.33 |       | 2.99 |      |         |
| -0.82 | 0.141 | 0.012 | 0.102 | 0.079 | 0.38 | 0.42 | 3.02 | 2.81 | 0.2871 |
| -0.76 | 0.145 | 0.006 | 0.104 | 0.077 | 0.08 | 0.27 | 2.84 | 2.53 | 0.2092 |
| -0.76 | 0.157 | 0.016 | 0.106 | 0.089 | 0.13 | 0.17 | 2.86 | 2.61 | -0.1668 |
| -0.71 | 0.166 | 0.028 | 0.106 | 0.094 | 0.20 | 0.18 | 2.89 | 2.65 | 0.2479 |
| -0.71 | 0.156 | 0.015 | 0.115 | 0.083 | 0.23 | 0.23 | 2.74 | 2.55 | 0.0438 |
| -0.65 | 0.177 | 0.029 | 0.113 | 0.096 | 0.18 | 0.23 | 2.71 | 2.59 | 0.5678 |
| -0.65 | 0.166 | 0.012 | 0.114 | 0.088 | 0.19 | 0.14 | 2.71 | 2.48 | 0.2266 |
| -0.60 | 0.193 | 0.031 | 0.114 | 0.103 | 0.24 | 0.12 | 2.88 | 2.65 | -0.1070 |
| -0.57 | 0.191 | 0.009 | 0.124 | 0.083 | 0.25 | 0.04 | 2.68 | 2.36 | 0.8261 |
| -0.53 | 0.205 | 0.026 | 0.118 | 0.107. | 0.33 | 0.14 | 3.17 | 2.56 | 0.1100 |
| -0.53 | 0.200 | 0.015 | 0.123 | 0.089 | 0.16 | 0.21 | 2.58 | 2.53 | 0.8239 |
| -0.48 | 0.219 | 0.027 | 0.121 | 0.105 | 0.10 | 0.16 | 2.72 | 2.52 | 0.3221 |
| -0.47 | 0.211 | 0.013 | 0.127 | 0.089 | 0.29 | 0.27 | 2.84 | 2.59 | -0.0120 |
| -0.42 | 0.219 | 0.013 | 0.128 | 0.098 | 0.23 | 0.23 | 2.66 | 2.69 | 0.7674 |
| -0.42 | 0.229 | 0.020 | 0.127 | 0.103 | 0.33 | 0.21 | 2.79 | 2.35 | 0.5128 |
| -0.36 | 0.237 | 0.015 | 0.127 | 0.092 | 0.37 | 0.11 | 2.96 | 2.50 | 0.0540 |
| -0.36 | 0.239 | 0.022 | 0.121 | 0.111 | 0.19 | 0.20 | 2.86 | 2.50 | 0.3241 |
| -0.31 | 0.250 | 0.020 | 0.125 | 0.119 | 0.27 | -0.07 | 2.80 | 2.67 | -0.5854 |
| -0.30 | 0.249 | 0.015 | 0.127 | 0.094 | 0.09 | 0.23 | 2.69 | 2.44 | 0.4096 |
| -0.25 | 0.258 | 0.010 | 0.131 | 0.095 | 0.23 | 0.09 | 2.85 | 2.59 | 0.5807 |
| -0.25 | 0.264 | 0.018 | 0.132 | 0.113 | 0.21 | 0.02 | 2.73 | 2.53 | 0.6527 |
| -0.19 | 0.273 | 0.007 | 0.130 | 0.113 | 0.23 | 0.13 | 2.97 | 2.48 | 0.8699 |

## Table A-1. Continued

LV DATA FOR X/D = 4.01                    — REACTING —

| R/RD | U/UP | V/UP | U'/UP | V'/UP | S AXIAL | S RADIAL | K AXIAL | K RADIAL | $\overline{U'V'}/UP^2$ (× 1,000) |
|---|---|---|---|---|---|---|---|---|---|
| -0.19 | 0.276 | 0.011 | 0.133 | 0.095 | 0.24 | -0.03 | 2.75 | 2.45 | 0.4482 |
| -0.13 | 0.282 | 0.006 | 0.131 | 0.106 | 0.26 | 0.01 | 2.80 | 2.40 | 0.2786 |
| -0.13 | 0.277 | 0.010 | 0.136 | 0.100 | 0.26 | -0.02 | 2.67 | 2.53 | 0.0218 |
| -0.08 | 0.285 | 0.004 | 0.128 | 0.095 | 0.27 | -0.05 | 2.62 | 2.50 | -0.1972 |
| -0.07 | 0.281 | 0.010 | 0.128 | 0.114 | 0.28 | 0.02 | 2.91 | 2.49 | 0.4385 |
| -0.02 | 0.285 | -0.000 | 0.133 | 0.093 | 0.24 | 0.07 | 2.74 | 2.58 | -0.3597 |
| -0.02 | 0.287 | -0.002 | 0.132 | 0.113 | 0.22 | -0.05 | 2.87 | 2.53 | -0.0640 |
| -0.00 | 0.279 | -0.004 | 0.130 | 0.111 | 0.27 | 0.04 | 3.07 | 2.53 | 0.5537 |
| 0.00 | 0.294 | -0.000 | 0.136 | 0.090 | 0.30 | 0.06 | 2.85 | 2.69 | 0.1795 |
| 0.02 | 0.272 | -0.003 | 0.128 | 0.115 | 0.21 | -0.11 | 2.60 | 2.62 | -0.5570 |
| 0.02 | 0.282 | 0.002 | 0.130 | 0.094 | 0.27 | -0.03 | 2.74 | 2.62 | -0.1533 |
| 0.04 | 0.273 | 0.005 | 0.130 | 0.111 | 0.27 | 0.05 | 2.93 | 2.51 | 0.4021 |
| 0.07 | 0.282 | 0.006 | 0.132 | 0.094 | 0.30 | 0.06 | 2.86 | 2.48 | -0.1562 |
| 0.10 | 0.277 | 0.012 | 0.135 | 0.110 | 0.22 | -0.02 | 2.49 | 2.56 | 0.5550 |
| 0.14 | 0.265 | 0.005 | 0.130 | 0.096 | 0.22 | -0.05 | 2.71 | 2.54 | -0.2287 |
| 0.15 | 0.260 | 0.013 | 0.130 | 0.115 | 0.27 | -0.16 | 2.83 | 2.97 | 0.2562 |
| 0.19 | 0.264 | 0.003 | 0.130 | 0.092 | 0.26 | 0.04 | 2.79 | 2.45 | -0.2819 |
| 0.21 | 0.261 | 0.015 | 0.129 | 0.111 | 0.31 | 0.07 | 3.15 | 2.47 | -0.2263 |
| 0.25 | 0.258 | 0.016 | 0.120 | 0.093 | 0.21 | 0.14 | 2.71 | 2.72 | 0.1501 |
| 0.27 | 0.256 | 0.017 | 0.128 | 0.108 | 0.29 | 0.09 | 2.96 | 2.55 | 0.3656 |
| 0.30 | 0.243 | 0.015 | 0.125 | 0.094 | 0.30 | 0.06 | 2.78 | 2.58 | 0.6400 |
| 0.30 | 0.244 | 0.008 | 0.123 | 0.089 | 0.26 | 0.03 | 2.61 | 2.46 | 0.3709 |
| 0.33 | 0.248 | 0.026 | 0.132 | 0.109 | 0.26 | 0.03 | 2.69 | 2.51 | 0.7251 |
| 0.36 | 0.235 | 0.027 | 0.119 | 0.086 | 0.29 | 0.26 | 2.55 | 2.57 | 0.4845 |
| 0.39 | 0.227 | 0.025 | 0.126 | 0.104 | 0.26 | 0.12 | 2.82 | 2.57 | 0.5384 |
| 0.42 | 0.219 | 0.019 | 0.122 | 0.091 | 0.22 | 0.15 | 2.73 | 2.42 | 0.2923 |
| 0.44 | 0.119 | | 0.099 | | 0.18 | | 2.76 | | |

## Table A-1. Continued

LV DATA FOR X/D = 5.01                    — REACTING —

| R/RD | U/UP | V/UP | U'/UP | V'/UP | S AXIAL | S RADIAL | K AXIAL | K RADIAL | $\overline{u'v'}/UP^2$ (x 1,000) |
|---|---|---|---|---|---|---|---|---|---|
| -0.93 | 0.153 | 0.071 | 0.100 | 0.166 | -0.07 | 0.70 | 2.14 | 2.79 | 4.2182 |
| -0.93 | 0.137 |  | 0.072 |  | 0.14 |  | 2.85 |  |  |
| -0.93 | 0.144 | 0.004 | 0.076 | 0.029 | -0.05 | 0.19 | 2.42 | 2.53 | 0.2518 |
| -0.89 | 0.152 | -0.000 | 0.074 | 0.045 | 0.32 | 0.27 | 2.94 | 2.80 | -0.0794 |
| -0.82 | 0.137 | 0.003 | 0.071 | 0.031 | 0.36 | 0.17 | 2.80 | 2.07 | 0.3103 |
| -0.82 | 0.154 | -0.001 | 0.073 | 0.051 | 0.27 | 0.37 | 2.82 | 2.89 | -0.0418 |
| -0.78 | 0.150 | 0.001 | 0.077 | 0.038 | 0.27 | 0.07 | 2.78 | 2.06 | 0.2062 |
| -0.76 | 0.165 | 0.002 | 0.088 | 0.055 | 0.80 | 0.25 | 4.30 | 2.96 | 0.2015 |
| -0.74 | 0.141 | 0.003 | 0.071 | 0.042 | 0.20 | -0.09 | 2.58 | 2.43 | 0.2779 |
| -0.71 | 0.158 | 0.003 | 0.074 | 0.058 | 0.34 | 0.17 | 2.87 | 3.00 | -0.0467 |
| -0.68 | 0.146 | 0.007 | 0.073 | 0.042 | 0.07 | 0.15 | 2.57 | 2.25 | 0.3007 |
| -0.65 | 0.161 | 0.006 | 0.075 | 0.060 | 0.27 | 0.18 | 2.82 | 2.65 | 0.0579 |
| -0.62 | 0.154 | 0.008 | 0.081 | 0.051 | 0.13 | -0.08 | 2.55 | 2.30 | 0.5630 |
| -0.59 | 0.165 | 0.005 | 0.074 | 0.061 | 0.30 | 0.30 | 2.84 | 2.86 | -0.0153 |
| -0.56 | 0.155 | 0.005 | 0.078 | 0.051 | 0.28 | 0.17 | 2.68 | 2.26 | 0.4070 |
| -0.53 | 0.178 | 0.007 | 0.088 | 0.065 | 0.66 | 0.20 | 4.08 | 2.61 | -0.0375 |
| -0.51 | 0.157 | 0.008 | 0.077 | 0.053 | 0.21 | 0.14 | 2.75 | 2.42 | 0.1760 |
| -0.48 | 0.180 | 0.007 | 0.090 | 0.065 | 0.62 | 0.21 | 3.83 | 2.81 | -0.1087 |
| -0.45 | 0.162 | -0.002 | 0.078 | 0.053 | 0.10 | 0.10 | 2.93 | 2.72 | 0.1726 |
| -0.42 | 0.176 | 0.005 | 0.082 | 0.067 | 0.33 | 0.16 | 3.18 | 2.66 | -0.0252 |
| -0.39 | 0.169 | -0.000 | 0.075 | 0.056 | 0.11 | 0.10 | 2.60 | 2.35 | 0.0335 |
| -0.37 | 0.176 | 0.007 | 0.077 | 0.067 | 0.22 | 0.08 | 2.94 | 2.77 | 0.2443 |
| -0.34 | 0.167 | 0.007 | 0.086 | 0.057 | 0.49 | -0.01 | 3.05 | 2.92 | 0.2354 |
| -0.31 | 0.175 | 0.005 | 0.077 | 0.066 | 0.33 | 0.20 | 2.77 | 2.73 | 0.0774 |
| -0.28 | 0.181 | 0.007 | 0.083 | 0.057 | 0.26 | -0.01 | 2.44 | 2.56 | 0.5919 |
| -0.24 | 0.181 | 0.004 | 0.080 | 0.069 | 0.21 | 0.02 | 2.96 | 2.69 | -0.0364 |
| -0.23 | 0.176 | 0.007 | 0.078 | 0.058 | 0.17 | -0.01 | 2.59 | 2.24 | 0.0449 |

## Table A-1. Continued

LV DATA FOR X/D = 5.01                    — REACTING —

| R/RD | U/UP | V/UP | U'/UP | V'/UP | S AXIAL | S RADIAL | K AXIAL | K RADIAL | $\overline{U'V'}/UP^2$ (× 1,000) |
|------|------|------|-------|-------|---------|----------|---------|----------|------------------|
| -0.19 | 0.183 | -0.000 | 0.079 | 0.066 | 0.27 | 0.06 | 3.06 | 2.70 | 0.0659 |
| -0.16 | 0.181 | 0.011 | 0.086 | 0.060 | 0.14 | -0.00 | 2.64 | 2.35 | -0.0524 |
| -0.13 | 0.178 | -0.000 | 0.081 | 0.069 | 0.27 | 0.14 | 2.97 | 2.69 | -0.0492 |
| -0.11 | 0.183 | 0.004 | 0.085 | 0.061 | 0.13 | -0.07 | 2.89 | 2.62 | 0.3867 |
| -0.08 | 0.183 | 0.001 | 0.078 | 0.068 | 0.41 | 0.03 | 3.46 | 2.66 | -0.0601 |
| -0.05 | 0.187 | -0.000 | 0.081 | 0.057 | 0.21 | -0.03 | 2.62 | 2.41 | 0.2052 |
| -0.02 | 0.182 | 0.003 | 0.082 | 0.068 | 0.26 | -0.05 | 2.74 | 2.67 | -0.1772 |
| -0.00 | 0.184 | 0.001 | 0.078 | 0.068 | 0.21 | 0.10 | 2.89 | 2.82 | -0.1743 |
| 0.01 | 0.185 | 0.000 | 0.087 | 0.057 | 0.21 | 0.05 | 2.62 | 2.74 | -0.0018 |
| 0.02 | 0.182 | 0.005 | 0.078 | 0.067 | 0.30 | -0.02 | 2.90 | 2.65 | -0.1521 |
| 0.03 | 0.174 | 0.006 | 0.078 | 0.057 | 0.09 | -0.00 | 2.57 | 2.38 | -0.0671 |
| 0.04 | 0.185 | 0.002 | 0.080 | 0.069 | 0.27 | 0.11 | 2.96 | 2.70 | -0.0259 |
| 0.05 | 0.177 | -0.003 | 0.079 | 0.053 | 0.37 | 0.22 | 3.57 | 2.51 | 0.1907 |
| 0.10 | 0.182 | 0.003 | 0.078 | 0.067 | 0.26 | 0.11 | 2.87 | 2.77 | 0.2111 |
| 0.10 | 0.180 | -0.001 | 0.084 | 0.053 | 0.28 | 0.14 | 2.73 | 2.31 | 0.2637 |
| 0.15 | 0.180 | 0.005 | 0.079 | 0.066 | 0.19 | -0.03 | 2.67 | 2.70 | 0.1363 |
| 0.16 | 0.175 | 0.005 | 0.074 | 0.059 | 0.17 | -0.02 | 2.96 | 2.32 | -0.1719 |
| 0.21 | 0.181 | 0.007 | 0.079 | 0.065 | 0.42 | 0.12 | 3.30 | 2.74 | 0.1660 |
| 0.22 | 0.173 | 0.003 | 0.078 | 0.057 | 0.15 | 0.23 | 2.80 | 2.57 | -0.2554 |
| 0.27 | 0.173 | 0.007 | 0.077 | 0.067 | 0.28 | 0.09 | 3.00 | 2.65 | -0.0870 |
| 0.28 | 0.169 | 0.010 | 0.079 | 0.057 | 0.25 | 0.16 | 2.98 | 2.70 | -0.0958 |
| 0.32 | 0.175 | 0.009 | 0.078 | 0.069 | 0.36 | 0.07 | 3.13 | 2.92 | -0.0327 |
| 0.33 | 0.167 | 0.009 | 0.075 | 0.057 | 0.12 | 0.20 | 2.65 | 2.48 | 0.1265 |
| 0.38 | 0.167 | 0.009 | 0.076 | 0.067 | 0.31 | 0.05 | 3.06 | 2.88 | -0.0513 |
| 0.39 | 0.159 | 0.006 | 0.072 | 0.053 | 0.23 | 0.20 | 2.81 | 2.46 | 0.1002 |
| 0.44 | 0.141 |  | 0.070 |  | 0.33 |  | 3.03 |  |  |
| 0.44 | 0.153 | 0.007 | 0.072 | 0.057 | 0.26 | 0.08 | 2.50 | 2.11 | 0.1178 |

## Table A-1. Continued

LV DATA FOR X/D – 6.01          – REACTING –

| R/RD | U/UP | V/UP | U'/UP | V'/UP | S AXIAL | S RADIAL | K AXIAL | K RADIAL | $\overline{U'V'}/UP^2$ (x 1,000) |
|---|---|---|---|---|---|---|---|---|---|
| -0.94 | 0.135 | 0.011 | 0.054 | 0.065 | -0.25 | -0.72 | 2.66 | 3.88 | -0.7618 |
| -0.89 | 0.149 | -0.001 | 0.058 | 0.030 | 0.19 | 0.18 | 3.14 | 3.14 | 0.1265 |
| -0.81 | 0.154 | -0.002 | 0.059 | 0.035 | 0.16 | 0.44 | 2.97 | 3.46 | 0.0155 |
| -0.76 | 0.149 | -0.002 | 0.058 | 0.036 | 0.30 | 0.19 | 3.10 | 3.13 | 0.0034 |
| -0.70 | 0.153 | -0.001 | 0.056 | 0.038 | 0.29 | 0.18 | 2.90 | 2.96 | 0.0207 |
| -0.65 | 0.152 | 0.001 | 0.053 | 0.040 | 0.24 | 0.03 | 3.14 | 3.16 | -0.0403 |
| -0.60 | 0.150 | 0.001 | 0.054 | 0.041 | 0.12 | 0.14 | 2.90 | 2.87 | -0.0100 |
| -0.54 | 0.149 | 0.001 | 0.055 | 0.043 | 0.22 | 0.12 | 3.15 | 2.87 | 0.0095 |
| -0.48 | 0.150 | 0.002 | 0.054 | 0.043 | 0.14 | 0.24 | 3.12 | 2.78 | 0.0203 |
| -0.42 | 0.145 | 0.001 | 0.054 | 0.043 | 0.15 | -0.01 | 2.87 | 2.77 | 0.1544 |
| -0.36 | 0.148 | 0.003 | 0.054 | 0.044 | 0.27 | -0.01 | 3.07 | 2.83 | -0.0979 |
| -0.31 | 0.149 | 0.001 | 0.056 | 0.045 | 0.27 | 0.04 | 3.26 | 2.71 | -0.0411 |
| -0.25 | 0.149 | 0.002 | 0.054 | 0.046 | 0.16 | -0.03 | 3.09 | 2.67 | 0.1087 |
| -0.19 | 0.149 | 0.000 | 0.057 | 0.044 | 0.13 | 0.04 | 3.04 | 2.58 | 0.0319 |
| -0.13 | 0.147 | -0.000 | 0.054 | 0.047 | 0.18 | 0.07 | 2.95 | 2.90 | -0.0501 |
| -0.07 | 0.145 | 0.004 | 0.053 | 0.060 | 0.26 | 1.87 | 3.19 | 12.41 | 0.0261 |
| 0.00 | 0.152 | -0.001 | 0.053 | 0.044 | 0.18 | 0.12 | 2.76 | 2.56 | 0.0284 |
| 0.02 | 0.151 | 0.001 | 0.054 | 0.043 | 0.27 | -0.00 | 2.79 | 2.47 | -0.0522 |
| 0.04 | 0.150 | 0.001 | 0.053 | 0.041 | 0.16 | 0.05 | 2.78 | 2.40 | 0.0567 |
| 0.10 | 0.149 | 0.000 | 0.055 | 0.043 | 0.10 | 0.06 | 2.76 | 2.26 | -0.0128 |
| 0.15 | 0.146 | 0.003 | 0.051 | 0.041 | 0.18 | 0.10 | 2.68 | 2.40 | -0.0033 |
| 0.21 | 0.144 | 0.002 | 0.051 | 0.043 | 0.14 | 0.03 | 2.62 | 2.47 | 0.0530 |
| 0.27 | 0.142 | 0.000 | 0.052 | 0.041 | 0.09 | 0.17 | 2.72 | 2.42 | -0.0706 |
| 0.32 | 0.147 | 0.001 | 0.051 | 0.040 | 0.08 | 0.24 | 2.69 | 2.31 | 0.0679 |
| 0.33 | 0.151 | 0.002 | 0.052 | 0.041 | -0.06 | 0.21 | 2.52 | 2.40 | -0.1466 |
| 0.44 | 0.129 | | 0.055 | | 0.23 | | 2.97 | | |

## Table A-1. Continued

LV DATA FOR X/D – 0.10                    – NONREACTING –

| R/RD | U/UP | V/UP | U'/UP | V'/UP | S AXIAL | S RADIAL | K AXIAL | K RADIAL | $\overline{U'V'}/UP^2$ (× 1,000) |
|------|------|------|-------|-------|---------|----------|---------|----------|--------------------------------|
| -0.36 | 0.759 | 0.014 | 0.125 | 0.064 | -0.01 | -0.46 | 2.73 | 3.19 | 0.1752 |
| -0.33 | 0.962 | -0.002 | 0.100 | 0.049 | -0.21 | -0.14 | 2.78 | 2.80 | 0.1815 |
| -0.24 | 1.014 | 0.001 | 0.113 | 0.044 | -1.10 | -0.11 | 5.00 | 2.72 | 0.1836 |
| -0.19 | 1.079 | 0.004 | 0.074 | 0.040 | -0.31 | -0.19 | 2.91 | 2.95 | 0.1067 |
| -0.13 | 1.107 | 0.005 | 0.067 | 0.036 | -0.26 | -0.14 | 3.15 | 2.79 | 0.1193 |
| -0.08 | 1.093 | 0.002 | 0.113 | 0.037 | -2.17 | -0.06 | 9.13 | 2.96 | 0.0417 |
| -0.02 | 1.094 | -0.000 | 0.106 | 0.038 | -2.07 | -0.12 | 8.48 | 2.88 | 0.0615 |
| 0.04 | 1.110 | -0.001 | 0.057 | 0.037 | -0.09 | -0.08 | 3.04 | 3.17 | 0.0744 |
| 0.06 | 1.097 | -0.001 | 0.060 | 0.038 | -0.10 | -0.10 | 2.75 | 2.95 | -0.0009 |
| 0.07 | 1.111 | 0.001 | 0.065 | 0.037 | -0.25 | -0.13 | 3.04 | 2.84 | -0.0438 |
| 0.08 | 1.096 | -0.003 | 0.063 | 0.039 | -0.20 | -0.13 | 3.00 | 3.37 | -0.0371 |
| 0.10 | 1.100 | -0.003 | 0.065 | 0.039 | -0.15 | -0.07 | 2.92 | 3.05 | -0.0569 |
| 0.16 | 1.059 | -0.002 | 0.074 | 0.041 | -0.30 | -0.13 | 3.14 | 2.77 | 0.0925 |
| 0.21 | 1.020 | -0.002 | 0.077 | 0.042 | -0.22 | -0.14 | 2.87 | 2.70 | -0.0261 |
| 0.27 | 0.577 | -0.005 | 0.088 | 0.045 | -0.17 | -0.18 | 2.60 | 2.72 | 0.0187 |
| 0.33 | 0.891 | 0.002 | 0.094 | 0.044 | -0.19 | 0.13 | 2.70 | 2.55 | 0.0837 |
| 0.38 | 0.740 | 0.009 | 0.123 | 0.054 | -0.18 | -0.29 | 2.93 | 3.34 | 0.3397 |

## Table A-1. Continued

LV DATA FOR X/D = 0.50                — NONREACTING —

| R/RD | U/UP | V/UP | U'/UP | V'/UP | S AXIAL | S RADIAL | K AXIAL | K RADIAL | $\overline{U'V'}/UP^2$ (× 1,000) |
|------|------|------|-------|-------|---------|----------|---------|----------|-------------------|
| −0.46 | 0.543 | 0.100 | 0.168 | 0.095 | −0.52 | −0.85 | 2.87 | 3.57 | 1.4164 |
| −0.40 | 0.733 | 0.070 | 0.144 | 0.072 | −0.70 | −0.90 | 3.48 | 4.03 | 0.9407 |
| −0.35 | 0.866 | 0.034 | 0.105 | 0.048 | −0.38 | −0.38 | 3.28 | 3.33 | 0.4877 |
| −0.29 | 0.958 | 0.005 | 0.093 | 0.048 | −0.30 | −0.29 | 2.70 | 2.92 | 0.2531 |
| −0.24 | 1.007 | −0.006 | 0.085 | 0.048 | −0.28 | −0.21 | 2.87 | 3.01 | 0.1139 |
| −0.17 | 1.071 | 0.003 | 0.073 | 0.042 | −0.21 | −0.10 | 2.84 | 2.90 | 0.1326 |
| −0.12 | 1.097 | 0.000 | 0.067 | 0.039 | −0.26 | −0.23 | 2.95 | 2.95 | 0.1052 |
| −0.06 | 1.112 | −0.001 | 0.061 | 0.037 | −0.22 | −0.18 | 3.02 | 3.09 | 0.0031 |
| −0.00 | 1.131 | 0.000 | 0.060 | 0.037 | −0.30 | −0.13 | 3.04 | 2.92 | −0.0325 |
| 0.05 | 1.120 | −0.000 | 0.066 | 0.036 | −0.24 | −0.01 | 3.07 | 3.08 | 0.0356 |
| 0.07 | 1.113 | 0.000 | 0.062 | 0.038 | −0.27 | 0.00 | 2.77 | 2.84 | 0.0358 |
| 0.09 | 1.107 | −0.000 | 0.065 | 0.039 | −0.23 | −0.09 | 3.03 | 3.14 | 0.0488 |
| 0.11 | 1.095 | −0.005 | 0.070 | 0.040 | −0.19 | −0.18 | 3.13 | 3.29 | −0.0969 |
| 0.17 | 1.055 | −0.001 | 0.078 | 0.042 | −0.31 | −0.13 | 2.93 | 2.75 | 0.0332 |
| 0.23 | 1.016 | −0.001 | 0.081 | 0.046 | −0.24 | −0.14 | 2.99 | 3.12 | 0.0716 |
| 0.28 | 0.971 | 0.001 | 0.090 | 0.049 | −0.24 | −0.08 | 2.82 | 2.88 | 0.1276 |
| 0.34 | 0.901 | 0.011 | 0.094 | 0.049 | −0.13 | −0.04 | 2.79 | 3.08 | −0.1374 |
| 0.40 | 0.789 | 0.033 | 0.125 | 0.072 | −0.59 | −0.99 | 3.46 | 4.41 | 0.3343 |
| 0.45 | 0.596 | 0.059 | 0.184 | 0.112 | −0.53 | −0.87 | 2.86 | 3.42 | 0.6287 |
| 0.51 | 0.340 | 0.061 | 0.234 | 0.139 | −0.41 | −0.56 | 2.72 | 2.39 | 1.9491 |

## Table A-1. Continued

LV DATA FOR X/D = 1.00                   – NONREACTING –

| R/RD | U/UP | V/UP | U'/UP | V'/UP | S AXIAL | S RADIAL | K AXIAL | K RADIAL | $\overline{u'v'}/UP^2$ (x 1,000) |
|---|---|---|---|---|---|---|---|---|---|
| -0.62 | 0.408 | 0.062 | 0.225 | 0.121 | -0.67 | -0.67 | 3.09 | 2.75 | 0.7009 |
| -0.53 | 0.592 | 0.040 | 0.221 | 0.109 | -0.90 | -0.75 | 3.41 | 3.24 | 1.5616 |
| -0.52 | 0.567 | 0.085 | 0.177 | 0.117 | -0.83 | -0.73 | 3.62 | 3.25 | 1.0864 |
| -0.41 | 0.831 | 0.024 | 0.140 | 0.075 | -0.94 | -0.99 | 3.87 | 4.47 | 0.9949 |
| -0.41 | 0.800 | 0.047 | 0.128 | 0.081 | -0.86 | -0.78 | 4.01 | 3.93 | 0.2503 |
| -0.30 | 0.990 | 0.013 | 0.082 | 0.046 | -0.06 | -0.23 | 2.82 | 3.13 | 0.1138 |
| -0.29 | 0.954 | 0.023 | 0.084 | 0.050 | -0.14 | -0.17 | 2.87 | 3.16 | -0.0212 |
| -0.18 | 1.083 | -0.001 | 0.077 | 0.043 | -0.18 | -0.18 | 2.73 | 3.03 | 0.1947 |
| -0.18 | 1.040 | 0.002 | 0.083 | 0.044 | -0.24 | -0.07 | 2.82 | 2.81 | 0.0497 |
| -0.07 | 1.139 | -0.002 | 0.062 | 0.036 | -0.22 | -0.08 | 2.74 | 2.71 | -0.0472 |
| -0.07 | 1.097 | -0.007 | 0.078 | 0.053 | -0.32 | -0.00 | 2.84 | 2.74 | 0.0559 |
| 0.01 | 1.121 | 0.003 | 0.070 | 0.050 | -0.20 | 0.11 | 2.91 | 2.98 | -0.2354 |
| 0.03 | 1.167 | 0.003 | 0.069 | 0.039 | -0.34 | -0.21 | 3.42 | 3.18 | -0.0532 |
| 0.05 | 1.139 | -0.001 | 0.061 | 0.038 | -0.21 | -0.06 | 3.09 | 2.67 | 0.0241 |
| 0.05 | 1.099 | 0.000 | 0.071 | 0.052 | -0.29 | -0.07 | 2.72 | 3.03 | 0.0152 |
| 0.09 | 1.131 | -0.001 | 0.063 | 0.039 | -0.32 | -0.07 | 3.03 | 3.18 | 0.0166 |
| 0.16 | 1.089 | -0.000 | 0.076 | 0.040 | -0.21 | 0.02 | 2.79 | 2.83 | -0.0658 |
| 0.16 | 1.047 | -0.002 | 0.081 | 0.048 | -0.26 | -0.17 | 2.74 | 2.87 | 0.4707 |
| 0.27 | 1.003 | 0.005 | 0.085 | 0.047 | -0.18 | -0.12 | 2.84 | 3.16 | 0.0576 |
| 0.28 | 0.960 | 0.008 | 0.097 | 0.058 | -0.21 | -0.18 | 3.02 | 2.96 | 0.6576 |
| 0.39 | 0.834 | 0.030 | 0.138 | 0.068 | -0.73 | -0.47 | 3.49 | 3.35 | 0.8969 |
| 0.39 | 0.748 | 0.023 | 0.003 | 0.001 | 0.21 | 0.15 | 1.98 | 2.11 | -0.0004 |
| 0.39 | 0.748 | 0.023 | 0.003 | 0.001 | 0.13 | 0.22 | 2.00 | 2.04 | -0.0002 |
| 0.39 | 0.724 | 0.040 | 0.176 | 0.094 | -0.72 | -0.32 | 3.12 | 2.56 | 1.8093 |
| 0.45 | 0.517 | 0.070 | 0.227 | 0.095 | -0.45 | -0.23 | 2.63 | 2.37 | 0.3804 |

## Table A-1. Continued

LV DATA FOR X/D = 2.00          — NONREACTING —

| R/RD | U/UP | V/UP | U'/UP | V'/UP | S AXIAL | S RADIAL | K AXIAL | K RADIAL | $\overline{U'V'}/UP^2$ (× 1,000) |
|------|------|------|-------|-------|---------|----------|---------|----------|------------------|
| -0.83 | -0.079 | 0.014 | 0.188 | 0.095 | 0.47 | 0.05 | 2.27 | 2.27 | 2.3438 |
| -0.79 | -0.031 | 0.024 | 0.214 | 0.118 | 0.34 | 0.23 | 2.13 | 2.26 | 5.7737 |
| -0.72 | 0.087 | 0.039 | 0.213 | 0.127 | -0.19 | 0.02 | 2.08 | 2.25 | 6.4699 |
| -0.67 | 0.206 | 0.039 | 0.234 | 0.134 | -0.34 | -0.18 | 2.55 | 2.14 | 6.5583 |
| -0.61 | 0.323 | 0.036 | 0.221 | 0.127 | -0.39 | -0.33 | 2.91 | 2.26 | 7.4618 |
| -0.55 | 0.439 | 0.040 | 0.211 | 0.120 | -0.50 | -0.40 | 3.04 | 2.66 | 4.8715 |
| -0.50 | 0.533 | 0.031 | 0.195 | 0.117 | -0.38 | -0.26 | 2.62 | 2.47 | 4.4896 |
| -0.44 | 0.668 | 0.024 | 0.175 | 0.104 | -0.78 | -0.54 | 3.43 | 3.05 | 2.6319 |
| -0.33 | 0.782 | 0.019 | 0.151 | 0.086 | -0.84 | -0.72 | 3.70 | 3.70 | 3.1396 |
| -0.33 | 0.874 | 0.019 | 0.110 | 0.066 | -0.62 | -0.59 | 3.50 | 3.70 | 1.0469 |
| -0.27 | 0.935 | 0.014 | 0.092 | 0.057 | -0.53 | -0.44 | 3.58 | 3.49 | 0.8690 |
| -0.21 | 0.975 | 0.006 | 0.077 | 0.047 | -0.17 | -0.13 | 3.30 | 2.92 | 0.4807 |
| -0.15 | 1.010 | 0.006 | 0.075 | 0.045 | -0.09 | -0.01 | 2.69 | 2.91 | 0.4615 |
| -0.10 | 1.039 | 0.004 | 0.070 | 0.043 | -0.10 | -0.03 | 2.84 | 2.96 | 0.2689 |
| -0.04 | 1.056 | 0.008 | 0.073 | 0.043 | -0.16 | 0.04 | 2.74 | 2.98 | 0.2269 |
| 0.02 | 1.077 | -0.006 | 0.067 | 0.045 | -0.25 | -0.09 | 2.93 | 2.84 | -0.1908 |
| 0.04 | 1.082 | 0.000 | 0.069 | 0.042 | -0.22 | 0.06 | 2.75 | 2.82 | 0.0516 |
| 0.05 | 1.065 | -0.003 | 0.072 | 0.044 | -0.33 | -0.05 | 2.95 | 2.79 | -0.0400 |
| 0.37 | 1.065 | -0.001 | 0.074 | 0.044 | -0.31 | -0.14 | 3.02 | 2.72 | 0.1162 |
| 0.13 | 1.055 | 0.001 | 0.077 | 0.047 | -0.28 | 0.05 | 2.79 | 2.95 | -0.0177 |
| 0.19 | 1.015 | 0.003 | 0.089 | 0.052 | -0.56 | -0.28 | 3.49 | 3.14 | 0.4685 |
| 0.25 | 0.999 | 0.009 | 0.102 | 0.054 | -0.84 | -0.28 | 4.48 | 3.28 | 0.3044 |
| 0.30 | 0.923 | 0.016 | 0.124 | 0.065 | -0.95 | -0.40 | 4.05 | 3.43 | 1.4333 |
| 0.37 | 0.845 | 0.028 | 0.159 | 0.079 | -0.92 | -0.23 | 3.83 | 2.97 | 1.7376 |
| 0.42 | 0.760 | 0.033 | 0.189 | 0.095 | -0.87 | -0.28 | 3.37 | 2.92 | 3.0493 |
| 0.48 | 0.622 | 0.032 | 0.221 | 0.122 | -0.61 | -0.36 | 2.81 | 2.76 | 6.4879 |

## Table A-1. Continued

LV DATA FOR X/D = 3.00         – NONREACTING –

| R/RD | U/UP | V/UP | U'/UP | V'/UP | S AXIAL | S RADIAL | K AXIAL | K RADIAL | $\overline{U'V'}/UP^2$ (× 1,000) |
|---|---|---|---|---|---|---|---|---|---|
| -0.87 | -0.182 | | 0.136 | | 0.99 | | 4.02 | | |
| -0.84 | -0.156 | 0.011 | 0.178 | 0.084 | 1.12 | 0.70 | 3.78 | 2.97 | 2.7296 |
| -0.78 | -0.107 | 0.017 | 0.210 | 0.109 | 0.78 | 0.42 | 2.78 | 2.60 | 4.4891 |
| -0.73 | -0.049 | 0.026 | 0.237 | 0.117 | 0.68 | 0.40 | 2.63 | 2.38 | 6.6678 |
| -0.67 | 0.032 | 0.022 | 0.249 | 0.131 | 0.29 | 0.33 | 2.06 | 2.25 | 8.0290 |
| -0.61 | 0.194 | 0.042 | 0.261 | 0.140 | -0.07 | -0.18 | 2.24 | 2.14 | 7.4885 |
| -0.55 | 0.297 | 0.030 | 0.276 | 0.143 | -0.15 | -0.10 | 2.45 | 2.10 | 7.4841 |
| -0.50 | 0.367 | 0.036 | 0.293 | 0.140 | -0.29 | -0.22 | 2.49 | 2.38 | 8.1474 |
| -0.44 | 0.492 | 0.014 | 0.279 | 0.132 | -0.45 | -0.33 | 2.54 | 2.42 | 8.3497 |
| -0.38 | 0.630 | 0.015 | 0.244 | 0.121 | -0.67 | -0.42 | 2.69 | 2.95 | 5.2292 |
| -0.32 | 0.779 | 0.015 | 0.204 | 0.086 | -1.20 | -0.61 | 4.11 | 3.19 | 2.9879 |
| -0.27 | 0.845 | 0.003 | 0.161 | 0.078 | -1.13 | -0.72 | 4.16 | 3.46 | 1.9200 |
| -0.21 | 0.955 | 0.002 | 0.108 | 0.064 | -0.79 | -0.68 | 3.90 | 3.61 | 0.4790 |
| -0.15 | 0.586 | 0.001 | 0.077 | 0.054 | -0.41 | -0.38 | 3.16 | 3.44 | 0.3782 |
| -0.10 | 1.027 | 0.008 | 0.072 | 0.050 | -0.25 | 0.04 | 3.39 | 3.60 | 0.2316 |
| -0.04 | 1.031 | -0.002 | 0.070 | 0.047 | -0.32 | -0.06 | 2.86 | 2.94 | -0.0007 |
| 0.02 | 1.042 | 0.003 | 0.070 | 0.050 | -0.18 | -0.20 | 3.01 | 3.27 | 0.1329 |
| 0.04 | 1.046 | 0.003 | 0.069 | 0.048 | -0.17 | -0.16 | 2.85 | 3.10 | -0.0269 |
| 0.05 | 1.041 | -0.001 | 0.071 | 0.048 | -0.42 | -0.07 | 3.69 | 3.11 | -0.1046 |
| 0.07 | 1.027 | -0.005 | 0.079 | 0.052 | -0.63 | -0.30 | 3.99 | 3.35 | 0.2122 |
| 0.13 | 0.995 | 0.003 | 0.095 | 0.061 | -0.96 | -0.39 | 4.66 | 3.48 | 0.3577 |
| 0.19 | 0.965 | 0.008 | 0.109 | 0.057 | -0.91 | -0.34 | 3.90 | 3.05 | 0.4968 |
| 0.25 | 0.903 | 0.000 | 0.155 | 0.075 | -1.03 | -0.61 | 3.75 | 3.35 | 0.7202 |
| 0.30 | 0.830 | 0.011 | 0.168 | 0.076 | -0.90 | -0.28 | 3.48 | 2.86 | 0.3860 |
| 0.36 | 0.762 | 0.005 | 0.225 | 0.110 | -0.57 | -0.60 | 2.80 | 2.95 | 0.6279 |
| 0.42 | 0.625 | 0.007 | 0.211 | 0.122 | -0.41 | -0.54 | 2.59 | 3.06 | 1.6833 |
| 0.48 | 0.548 | 0.010 | 0.218 | 0.131 | -0.19 | -0.28 | 2.41 | 2.54 | 0.4293 |

## Table A-1. Continued

LV DATA FOR X/D = 4.01  ·· NONREACTING –

| R/RD | U/UP | V/UP | U'/UP | V'/UP | S AXIAL | S RADIAL | K AXIAL | K RADIAL | $\overline{U'V'}/UP^2$ (× 1,000) |
|---|---|---|---|---|---|---|---|---|---|
| -0.93 | -0.095 | | 0.165 | | 0.72 | | 2.92 | | |
| -0.90 | -0.079 | 0.018 | 0.190 | 0.090 | 0.70 | 0.62 | 2.66 | 3.06 | 0.3846 |
| -0.84 | -0.004 | 0.037 | 0.224 | 0.128 | 0.38 | 0.32 | 2.24 | 2.42 | 2.0609 |
| -0.79 | 0.051 | 0.033 | 0.224 | 0.133 | 0.13 | 0.14 | 2.07 | 2.21 | 2.8123 |
| -0.72 | 0.093 | 0.035 | 0.237 | 0.131 | 0.20 | 0.08 | 2.30 | 2.12 | 2.1961 |
| -0.66 | 0.187 | 0.049 | 0.242 | 0.150 | 0.07 | -0.01 | 2.42 | 2.09 | 2.0922 |
| -0.61 | 0.218 | 0.026 | 0.259 | 0.149 | 0.04 | -0.05 | 2.42 | 2.07 | 1.4028 |
| -0.55 | 0.348 | 0.037 | 0.268 | 0.146 | -0.14 | -0.20 | 2.38 | 2.28 | 1.3072 |
| -0.49 | 0.381 | 0.044 | 0.264 | 0.158 | -0.19 | -0.16 | 2.68 | 2.12 | 0.9884 |
| -0.44 | 0.479 | 0.037 | 0.265 | 0.153 | -0.34 | -0.29 | 2.38 | 2.33 | 1.6310 |
| -0.38 | 0.610 | 0.023 | 0.254 | 0.122 | -0.60 | -0.52 | 2.74 | 2.93 | 2.3885 |
| -0.32 | 0.666 | 0.013 | 0.261 | 0.126 | -0.71 | -0.47 | 2.85 | 3.00 | 1.3569 |
| -0.26 | 0.775 | 0.010 | 0.226 | 0.112 | -1.03 | -0.56 | 3.38 | 3.43 | 0.8779 |
| -0.21 | 0.870 | 0.003 | 0.187 | 0.089 | -1.52 | -0.81 | 5.37 | 3.87 | 1.8215 |
| -0.15 | 0.922 | -0.000 | 0.153 | 0.081 | -1.77 | -0.37 | 6.81 | 3.40 | 1.0126 |
| -0.09 | 0.958 | -0.001 | 0.122 | 0.077 | -1.62 | -0.52 | 6.71 | 4.01 | 0.4283 |
| -0.04 | 0.983 | 0.000 | 0.093 | 0.073 | -1.17 | -0.01 | 5.52 | 3.95 | -0.0126 |
| -0.02 | 1.003 | 0.001 | 0.087 | 0.067 | -0.82 | -0.10 | 4.09 | 3.33 | 0.3031 |
| -0.00 | 0.989 | -0.000 | 0.090 | 0.061 | -1.29 | 0.14 | 5.95 | 3.15 | -0.0352 |
| 0.02 | 0.981 | 0.003 | 0.099 | 0.062 | -1.39 | -0.14 | 6.10 | 3.52 | 0.2279 |
| 0.07 | 0.944 | 0.002 | 0.121 | 0.071 | -1.41 | -0.28 | 5.74 | 3.37 | 0.1257 |
| 0.14 | 0.896 | -0.002 | 0.150 | 0.081 | -1.25 | -0.59 | 4.68 | 3.77 | 0.1151 |
| 0.19 | 0.848 | -0.000 | 0.162 | 0.090 | -1.01 | -0.78 | 3.79 | 3.78 | 0.5264 |
| 0.25 | 0.765 | -0.001 | 0.204 | 0.100 | -0.74 | -0.53 | 2.96 | 3.10 | 0.6479 |
| 0.31 | 0.686 | 0.006 | 0.196 | 0.112 | -0.55 | -0.54 | 2.72 | 3.00 | 1.9818 |
| 0.36 | 0.591 | -0.002 | 0.222 | 0.115 | -0.25 | -0.36 | 2.44 | 2.63 | 0.7045 |
| 0.42 | 0.497 | 0.005 | 0.208 | 0.131 | -0.12 | -0.49 | 2.42 | 2.80 | 2.4333 |

## Table A-1. Continued

LV DATA FOR X/D = 5.00        — NONREACTING —

| R/RD | U/UP | V/UP | U'/UP | V'/UP | S AXIAL | S RADIAL | K AXIAL | K RADIAL | $\overline{u'v'}/UP^2$ (x 1,000) |
|------|------|------|-------|-------|---------|----------|---------|----------|-------------------|
| -0.91 | 0.051 | 0.034 | 0.188 | 0.106 | 0.12 | 1.01 | 2.33 | 4.01 | 0.8063 |
| -0.84 | 0.132 | 0.045 | 0.157 | 0.131 | -0.07 | 0.30 | 2.45 | 2.40 | 0.7458 |
| -0.78 | 0.158 | 0.037 | 0.157 | 0.135 | -0.06 | 0.10 | 2.38 | 2.14 | 1.5210 |
| -0.72 | 0.199 | 0.049 | 0.208 | 0.138 | 0.06 | 0.01 | 2.67 | 2.17 | 1.6336 |
| -0.67 | 0.251 | 0.041 | 0.208 | 0.143 | 0.02 | -0.04 | 2.70 | 2.26 | 0.9593 |
| -0.61 | 0.313 | 0.042 | 0.207 | 0.141 | -0.06 | -0.10 | 2.69 | 2.16 | 0.3445 |
| -0.61 | 0.326 | 0.049 | 0.225 | 0.147 | -0.03 | -0.19 | 2.55 | 2.25 | 2.9721 |
| -0.55 | 0.382 | 0.039 | 0.221 | 0.140 | -0.04 | -0.18 | 2.52 | 2.17 | 2.1399 |
| -0.49 | 0.414 | 0.031 | 0.238 | 0.148 | -0.12 | -0.23 | 2.38 | 2.23 | 0.6678 |
| -0.44 | 0.450 | 0.026 | 0.236 | 0.147 | -0.02 | -0.17 | 2.28 | 2.25 | 1.6069 |
| -0.38 | 0.556 | 0.032 | 0.235 | 0.132 | -0.09 | -0.14 | 2.33 | 2.48 | -0.0259 |
| -0.32 | 0.630 | 0.031 | 0.231 | 0.131 | -0.42 | -0.29 | 2.54 | 2.56 | 1.7088 |
| -0.27 | 0.700 | 0.017 | 0.224 | 0.131 | -0.76 | -0.31 | 3.04 | 2.58 | 1.5710 |
| -0.21 | 0.727 | 0.015 | 0.222 | 0.134 | -0.79 | -0.27 | 2.89 | 2.83 | 2.1018 |
| -0.15 | 0.768 | 0.015 | 0.205 | 0.121 | -0.80 | -0.12 | 2.89 | 2.88 | -0.0043 |
| -0.10 | 0.841 | 0.004 | 0.182 | 0.111 | -1.01 | -0.21 | 3.60 | 2.78 | -0.1273 |
| -0.04 | 0.831 | -0.001 | 0.191 | 0.106 | -1.00 | 0.04 | 3.49 | 2.96 | 0.6266 |
| -0.02 | 0.864 | 0.012 | 0.157 | 0.115 | -0.88 | 0.27 | 3.39 | 3.37 | -0.0225 |
| -0.00 | 0.858 | 0.005 | 0.156 | 0.120 | -0.84 | 0.15 | 3.18 | 3.41 | 0.0170 |
| 0.02 | 0.850 | 0.003 | 0.165 | 0.114 | -1.04 | -0.12 | 3.87 | 3.22 | -0.4898 |
| 0.08 | 0.836 | 0.003 | 0.165 | 0.108 | -1.02 | -0.24 | 3.73 | 3.22 | 0.8895 |
| 0.13 | 0.804 | -0.002 | 0.185 | 0.115 | -0.77 | -0.30 | 2.98 | 2.95 | 0.2861 |
| 0.19 | 0.743 | 0.017 | 0.189 | 0.115 | -0.74 | -0.34 | 3.12 | 2.95 | 0.9812 |
| 0.25 | 0.713 | 0.012 | 0.202 | 0.120 | -0.67 | -0.47 | 2.84 | 2.98 | 1.4847 |
| 0.31 | 0.626 | 0.028 | 0.188 | 0.117 | -0.46 | -0.26 | 2.66 | 2.80 | 1.1693 |
| 0.36 | 0.572 | 0.028 | 0.201 | 0.121 | -0.26 | -0.33 | 2.37 | 2.68 | 1.1535 |
| 0.42 | 0.498 | 0.039 | 0.201 | 0.128 | -0.18 | -0.36 | 2.49 | 2.64 | -0.6580 |

# Table A-1. Concluded

LV DATA FOR X/D = 6.03      — NONREACTING —

| R/RD | U/UP | V/UP | U'/UP | V'/UP | S AXIAL | S RADIAL | K AXIAL | K RADIAL | $\overline{U'V'}/UP^2$ (× 1,000) |
|------|------|------|-------|-------|---------|----------|---------|----------|--------------------|
| -0.88 | 0.167 | -0.000 | 0.072 | 0.043 | -0.24 | -0.08 | 2.26 | 1.85 | -0.2536 |
| -0.82 | 0.402 | 0.015 | 0.088 | 0.106 | 1.03 | -0.04 | 3.82 | 1.86 | -0.0614 |
| -0.76 | 0.221 | 0.019 | 0.130 | 0.090 | -0.30 | -0.07 | 2.69 | 1.95 | 0.8310 |
| -0.72 | 0.269 | 0.031 | 0.149 | 0.111 | -0.13 | -0.17 | 2.61 | 2.05 | 0.5719 |
| -0.65 | 0.275 | 0.039 | 0.130 | 0.092 | -0.25 | 0.09 | 2.47 | 2.02 | 0.2364 |
| -0.59 | 0.328 | 0.012 | 0.150 | 0.104 | -0.10 | -0.07 | 2.16 | 2.58 | 0.2952 |
| -0.54 | 0.393 | 0.038 | 0.163 | 0.118 | -0.14 | -0.30 | 2.28 | 2.06 | 0.3930 |
| -0.49 | 0.423 | 0.020 | 0.182 | 0.112 | -0.09 | -0.33 | 2.30 | 2.18 | 0.7917 |
| -0.42 | 0.433 | 0.024 | 0.162 | 0.120 | -0.21 | -0.18 | 2.35 | 2.10 | 0.2682 |
| -0.36 | 0.507 | 0.018 | 0.174 | 0.111 | -0.26 | -0.33 | 2.27 | 2.29 | 1.3848 |
| -0.31 | 0.507 | 0.010 | 0.155 | 0.116 | -0.45 | -0.27 | 2.42 | 2.43 | 0.6073 |
| -0.25 | 0.611 | 0.022 | 0.193 | 0.110 | -0.32 | -0.31 | 2.41 | 2.25 | 0.8531 |
| -0.19 | 0.660 | 0.015 | 0.183 | 0.115 | -0.35 | -0.19 | 2.27 | 2.19 | 1.3126 |
| -0.19 | 0.648 | 0.032 | 0.196 | 0.125 | -0.30 | -0.21 | 2.39 | 2.50 | 0.8018 |
| -0.13 | 0.678 | -0.069 | 0.194 | 0.115 | -0.28 | -0.40 | 2.42 | 2.40 | 0.8640 |
| -0.07 | 0.716 | 0.010 | 0.179 | 0.111 | -0.40 | -0.03 | 2.42 | 2.30 | 0.0616 |
| -0.00 | 0.708 | -0.001 | 0.171 | 0.108 | -0.32 | -0.19 | 2.18 | 2.13 | 0.7903 |
| 0.00 | 0.688 | -0.007 | 0.163 | 0.121 | -0.43 | 0.07 | 2.62 | 2.90 | 0.6285 |
| 0.04 | 0.702 | 0.010 | 0.174 | 0.112 | -0.27 | 0.04 | 2.16 | 2.26 | 0.3825 |
| 0.15 | 0.673 | 0.012 | 0.176 | 0.110 | -0.12 | -0.01 | 2.15 | 2.28 | -0.8634 |
| 0.27 | 0.604 | 0.019 | 0.183 | 0.113 | -0.05 | -0.03 | 2.23 | 2.13 | 1.4706 |
| 0.33 | 0.517 | 0.032 | 0.187 | 0.121 | 0.07 | -0.02 | 2.23 | 2.10 | 1.6731 |
| 0.45 | 0.146 | 0.004 | 0.053 | 0.041 | 0.16 | 0.14 | 2.60 | 2.54 | -0.1017 |

### Table A-2. Nonreactive Hydrogen Mass Fraction and Total Pressure

| X/D | $R/R_D$ | $F_H$ | $P_T$ | X/D | $R/R_D$ | $F_H$ | $P_T$ |
|---|---|---|---|---|---|---|---|
| 0 | 0.03 | 0.001 | 14.79 | 2.0 | 0.02 | 0.0030 | 14.38 |
| | 0.09 | 0.001 | 14.77 | | 0.12 | 0.0030 | 14.18 |
| | 0.14 | 0.001 | 14.75 | | 0.24 | 0.0040 | 13.99 |
| | 0.19 | 0.001 | 14.72 | | 0.35 | 0.0050 | ---- |
| | 0.24 | 0.001 | 14.66 | | 0.46 | 0.0050 | 13.80 |
| | 0.29 | 0.001 | 14.54 | | 0.57 | 0.0060 | 13.71 |
| | 0.34 | 0.001 | 14.46 | | 0.67 | 0.0060 | 13.65 |
| | 0.39 | 0.002 | 14.24 | | 0.75 | 0.0050 | 13.62 |
| | 0.44 | 0.011 | 13.70 | | 0.83 | 0.0050. | 13.61 |
| | 0.49 | 0.024 | 13.51 | | 0.90 | 0.0060 | ---- |
| | 0.54 | 0.024 | 13.51 | | 1.00 | 0.0060 | 13.61 |
| | 0.60 | 0.028 | 13.51 | | | | |
| | 0.65 | 0.028 | 13.51 | 3.0 | 0.02 | 0.0047 | 13.95 |
| | 0.69 | 0.033 | 13.52 | | 0.13 | 0.0048 | 13.96 |
| | 0.74 | 0.029 | 13.52 | | 0.23 | 0.0048 | 13.87 |
| | 0.79 | 0.024 | 13.52 | | 0.33 | 0.0050 | 13.86 |
| | 0.84 | 0.028 | 13.53 | | 0.44 | 0.0051 | 13.80 |
| | 0.87 | 0.028 | 13.52 | | 0.53 | 0.0051 | 13.77 |
| | 0.93 | 0.028 | 13.52 | | 0.62 | 0.0050 | 13.73 |
| | 0.96 | 0.024 | 13.51 | | 0.73 | 0.0052 | 13.72 |
| | 1.00 | 0.020 | 13.51 | | 0.83 | 0.0050 | 13.71 |
| | | | | | 0.94 | 0.0053 | 13.71 |
| 0.5 | 0.03 | 0.001 | 14.78 | | 1.00 | 0.0052 | 13.68 |
| | 0.08 | 0.001 | 14.78 | | | | |
| | 0.13 | 0.001 | 14.73 | 4.0 | 0.02 | 0.0050 | 13.82 |
| | 0.23 | 0.001 | 14.64 | | 0.13 | 0.0050 | 13.82 |
| | 0.33 | 0.003 | 14.38 | | 0.23 | 0.0050 | 13.82 |
| | 0.45 | 0.008 | 13.80 | | 0.34 | 0.0050 | 13.80 |
| | 0.57 | 0.120 | 13.55 | | 0.43 | 0.0050 | 13.79 |
| | 0.67 | 0.120 | 13.52 | | 0.52 | 0.0049 | 13.80 |
| | 0.76 | 0.110 | 13.52 | | 0.63 | 0.0050 | 13.78 |
| | 0.81 | 0.120. | 13.51 | | 0.73 | 0.0050 | 13.77 |
| | 0.91 | 0.120 | 13.53 | | 0.81 | 0.0050 | 13.77 |
| | 1.00 | 0.150 | 13.55 | | 0.93 | 0.0050 | 13.77 |
| | | | | | 1.00 | 0.0050 | 13.76 |
| 1.0 | 0 | 0.002 | 14.74 | | | | |
| | 0.13 | 0.001 | 14.70 | 5.0 | 0.03 | 0.0050 | 13.78 |
| | 0.23 | 0.002 | 14.51 | | 0.12 | 0.0049 | 13.79 |
| | 0.32 | 0.004 | 14.18 | | 0.23 | 0.0050 | 13.78 |
| | 0.44 | 0.007 | 13.83 | | 0.33 | 0.0050 | 13.79 |
| | 0.54 | 0.007 | 13.63 | | 0.43 | 0,0050 | 13.79 |
| | 0.62 | 0.007 | 13.59 | | 0.53 | 0.0051 | 13.78 |
| | 0.75 | 0.007 | 13.53 | | 0.64 | 0.0050 | 13.78 |
| | 0.81 | 0.007 | 13.52 | | 0.73 | 0.0050 | 13.79 |
| | 0.90 | 0.008 | 13.54 | | 0.82 | 0.0050 | 13.80 |
| | 1.00 | 0.008 | 13.55 | | 0.90 | 0.0051 | 13.79 |
| | | | | | 1.00 | 0.0051 | 13.78 |
| | | | | | | | |
| | | | | 6.0 | 0.02 | 0.0050 | 13.78 |

Note: $P_T$ = psia

## Table A-3. Reactive Hydrogen Mass Fraction and Total Pressure

| $X/D$ | $R/R_D$ | $F_H$ | $X/D$ | $R/R_D$ | $F_H$ |
|---|---|---|---|---|---|
| 0 | 0.35 | 0 | 3.0 | 0.34 | 0.008 |
| | 0.42 | 0.023 | | 0.42 | 0.015 |
| | 0.45 | 0.025 | | 0.45 | 0.014 |
| | 0.51 | 0.022 | | 0.52 | 0.018 |
| | 0.57 | 0.021 | | 0.57 | 0.020 |
| | 0.64 | 0.024 | | 0.64 | 0.022 |
| | 0.70 | 0.015 | | 0.72 | 0.025 |
| | 0.77 | 0.019 | | 0.78 | 0.023 |
| | 0.90 | 0.019 | | 0.91 | 0.023 |
| | 0.99 | 0.029 | | 0.99 | 0.022 |
| 0.5 | 0.21 | 0 | 4.0 | 0.03 | 0.001 |
| | 0.26 | 0 | | 0.12 | 0.002 |
| | 0.35 | 0.005 | | 0.20 | 0.003 |
| | 0.42 | 0.021 | | 0.26 | 0.005 |
| | 0.46 | 0.029 | | 0.34 | 0.007 |
| | 0.52 | 0.034 | | 0.41 | 0.009 |
| | 0.58 | 0.032 | | 0.45 | 0.011 |
| | 0.71 | 0.032 | | 0.51 | 0.013 |
| | 0.79 | 0.030 | | 0.59 | 0.013 |
| | 0.89 | 0.033 | | 0.64 | 0.016 |
| | 0.99 | 0.031 | | 0.71 | 0.017 |
| | | | | 0.78 | 0.014 |
| 1.0 | 0.29 | 0.002 | | 0.89 | 0.017 |
| | 0.42 | 0.016 | | 0.99 | 0.017 |
| | 0.45 | 0.021 | | | | |
| | 0.50 | 0.035 | 5.0 | 0.02 | 0.003 |
| | 0.57 | 0.037 | | 0.06 | 0.003 |
| | 0.64 | 0.037 | | 0.18 | 0.004 |
| | 0.71 | 0.031 | | 0.27 | 0.006 |
| | 0.78 | 0.031 | | 0.34 | 0.007 |
| | 0.92 | 0.032 | | 0.41 | 0.008 |
| | 0.99 | 0.035 | | 0.44 | 0.009 |
| | | | | 0.51 | 0.009 |
| 2.0 | 0.19 | 0.001 | | 0.57 | 0.011 |
| | 0.27 | 0.002 | | 0.62 | 0.011 |
| | 0.34 | 0.006 | | 0.71 | 0.010 |
| | 0.41 | 0.011 | | 0.77 | 0.010 |
| | 0.46 | 0.015 | | 0.88 | 0.012 |
| | 0.52 | 0.024 | | 0.99 | 0.014 |
| | 0.57 | 0.027 | | | | |
| | 0.64 | 0.033 | 6.0 | 0.03 | 0.005 |
| | 0.71 | 0.037 | | 0.29 | 0.006 |
| | 0.78 | 0.036 | | 0.41 | 0.007 |
| | 0.90 | 0.036 | | 0.45 | 0.007 |
| | 0.99 | 0.035 | | 0.51 | 0.008 |
| | | | | 0.56 | 0.008 |
| 3.0 | 0.02 | 0 | | 0.62 | 0.008 |
| | 0.06 | 0.001 | | 0.70 | 0.009 |
| | 0.15 | 0.001 | | 0.78 | 0.009 |
| | 0.20 | 0.003 | | 0.90 | 0.009 |
| | 0.29 | 0.006 | | 0.99 | 0.009 |

## Table A-3. Continued

| X/D | R/R_D | P_T | X/D | R/R_D | P_T |
|-----|-------|-----|-----|-------|-----|
| 0 | 0 | 14.83 | 1.0 | 0.11 | 14.77 |
| | 0.04 | 14.83 | | 0.17 | 14.74 |
| | 0.08 | 14.82 | | 0.21 | 14.69 |
| | 0.13 | 14.81 | | 0.25 | 14.64 |
| | 0.17 | 14.78 | | 0.28 | 14.58 |
| | 0.22 | 14.72 | | 0.33 | 14.43 |
| | 0.27 | 14.65 | | 0.39 | 14.20 |
| | 0.30 | 14.61 | | 0.42 | 14.06 |
| | 0.35 | 14.49 | | 0.45 | 13.92 |
| | 0.38 | 14.38 | | 0.48 | 13.82 |
| | 0.41 | 14.22 | | 0.62 | 13.60 |
| | 0.44 | 13.88 | | 0.77 | 13.57 |
| | 0.46 | 13.62 | | 0.84 | 13.56 |
| | 0.48 | 13.57 | | 1.00 | 13.57 |
| | 0.54 | 13.56 | 2.0 | | |
| | 0.59 | 13.56 | | 0 | 14.78 |
| | 0.64 | 13.56 | | 0.04 | 14.77 |
| | 0.70 | 13.57 | | 0.09 | 14.75 |
| | 0.76 | 13.56 | | 0.16 | 14.69 |
| | 0.80 | 13.56 | | 0.23 | 14.56 |
| | 0.83 | 13.57 | | 0.30 | 14.34 |
| | 0.88 | 13.57 | | 0.33 | 14.28 |
| | 0.92 | 13.56 | | 0.39 | 14.04 |
| | 0.97 | 13.57 | | 0.45 | 13.89 |
| | 1.00 | 13.56 | | 0.49 | 13.83 |
| | | | | 0.56 | 13.71 |
| 0.5 | 0.01 | 14.82 | | 0.61 | 13.67 |
| | 0.07 | 14.82 | | 0.67 | 13.62 |
| | 0.12 | 14.81 | | 0.75 | 13.61 |
| | 0.17 | 14.77 | | 0.94 | 13.59 |
| | 0.23 | 14.72 | | 1.00 | 13.59 |
| | 0.29 | 14.64 | 3.0 | | |
| | 0.33 | 14.52 | | 0.01 | 14.68 |
| | 0.37 | 14.36 | | 0.04 | 14.70 |
| | 0.39 | 14.21 | | 0.07 | 14.63 |
| | 0.42 | 14.03 | | 0.13 | 14.56 |
| | 0.45 | 13.87 | | 0.18 | 14.46 |
| | 0.48 | 13.74 | | 0.22 | 14.37 |
| | 0.54 | 13.64 | | 0.27 | 14.21 |
| | 0.64 | 13.58 | | 0.31 | 14.14 |
| | 0.72 | 13.57 | | 0.36 | 14.01 |
| | 0.83 | 13.58 | | 0.40 | 13.92 |
| | 0.87 | 13.57 | | 0.44 | 13.83 |
| | 0.93 | 13.57 | | 0.52 | 13.73 |
| | 0.98 | 13.57 | | 0.63 | 13.67 |
| | | | | 0.70 | 13.67 |
| 1.0 | 0.02 | 14.80 | | 0.80 | 13.63 |
| 1.0 | 0.06 | 14.79 | | 0.94 | 13.62 |
| | | | | 1.00 | 13.63 |

Note: $P_T$ = psia

63

## Table A-3. Concluded

| X/D | R/R$_D$ | P$_T$ | X/D | R/R$_D$ | P$_T$ |
|-----|---------|-------|-----|---------|-------|
| 4.0 | 0.01 | 14.50 | 5.0 | 0.48 | 13.79 |
|     | 0.06 | 14.49 |     | 0.54 | 13.73 |
|     | 0.09 | 14.49 |     | 0.60 | 13.74 |
|     | 0.12 | 14.39 |     | 0.63 | 13.71 |
|     | 0.16 | 14.37 |     | 0.69 | 13.69 |
|     | 0.19 | 14.34 |     | 0.77 | 13.70 |
|     | 0.23 | 14.19 |     | 0.86 | 13.66 |
|     | 0.27 | 14.15 |     | 0.95 | 13.67 |
|     | 0.32 | 14.04 |     | 1.00 | 13.66 |
|     | 0.38 | 13.89 |     |      |       |
|     | 0.46 | 13.83 | 6.0 | 0.04 | 13.96 |
|     | 0.52 | 13.73 |     | 0.08 | 13.97 |
|     | 0.58 | 13.68 |     | 0.11 | 13.95 |
|     | 0.69 | 13.63 |     | 0.14 | 13.97 |
|     | 0.79 | 13.62 |     | 0.18 | 13.93 |
|     | 0.93 | 13.62 |     | 0.22 | 13.89 |
|     | 1.00 | 13.61 |     | 0.25 | 13.89 |
|     |      |       |     | 0.29 | 13.86 |
| 5.0 | 0.01 | 14.19 |     | 0.34 | 13.86 |
|     | 0.03 | 14.20 |     | 0.40 | 13.80 |
|     | 0.09 | 14.18 |     | 0.47 | 13.77 |
|     | 0.13 | 14.15 |     | 0.54 | 13.76 |
|     | 0.20 | 14.09 |     | 0.60 | 13.76 |
|     | 0.23 | 14.06 |     | 0.68 | 13.72 |
|     | 0.27 | 14.02 |     | 0.77 | 13.71 |
|     | 0.30 | 13.96 |     | 0.85 | 13.68 |
|     | 0.35 | 13.88 |     | 0.94 | 13.70 |
|     | 0.41 | 13.85 |     | 1.00 | 13.67 |

Note: $P_T$ = psia

64

## Table A-4. Wall Static Pressure Distribution

| X/D | Nonreactive $\Delta p$, psf | Reactive $\Delta p$, psf | X/D | Nonreactive $\Delta p$, psf | Reactive $\Delta p$, psf |
|---|---|---|---|---|---|
| 0 | 0 | 0 | 3.00 | 27.89 | 5.69 |
| 0.14 | −0.43 | 0 | 3.19 | 30.77 | 7.70 |
| 0.33 | −0.86 | 0 | 3.38 | 30.91 | 7.78 |
| 0.52 | −0.86 | 0 | 3.57 | 32.30 | 8.93 |
| 0.71 | −1.58 | 0 | 3.76 | 33.02 | 9.79 |
| 0.90 | −1.82 | 0 | 3.95 | 34.37 | 11.09 |
| 1.10 | −0.05 | 1.51 | 4.14 | 34.27 | 12.24 |
| 1.29 | 2.26 | 2.45 | 4.33 | 34.42 | 13.18 |
| 1.48 | 4.90 | 1.37 | 4.52 | 34.70 | 14.85 |
| 1.67 | 8.11 | 1.80 | 4.64 | 34.75 | 15.12 |
| 1.86 | 11.18 | 2.38 | 4.76 | 34.75 | 16.20 |
| 2.05 | 14.35 | 2.66 | 5.06 | 34.99 | 17.86 |
| 2.24 | 17.33 | 3.10 | 5.18 | 35.04 | 18.72 |
| 2.43 | 20.45 | 4.97 | 5.48 | 35.14 | 20.52 |
| 2.62 | 23.33 | 4.82 | 5.86 | 35.14 | 22.39 |
| 2.81 | 25.34 | 5.18 | 6.05 | 35.14 | 23.62 |

## Table A-5. Laser-Raman Temperature (°R)

| X/D | $R/R_D$ | $T_R$ | X/D | $R/R_D$ | $T_R$ |
|---|---|---|---|---|---|
| 0 | 0.02 | 574 | 3 | 0 | 626 |
| | 0.19 | 597 | | 0.10 | 596 |
| | 0.39 | 590 | | 0.20 | 578 |
| | 0.48 | 623 | | 0.29 | 727 |
| | 0.57 | 949 | | 0.39 | 745 |
| | 0.63 | 1,136 | | 0.47 | 994 |
| | 0.66 | 1,402 | | 0.56 | 1,346 |
| | 0.71 | 1,287 | | 0.66 | 1,100 |
| | 0.76 | 1,571 | | 0.77 | 1,496 |
| | 0.81 | 1,433 | | 0.85 | 1,514 |
| | 0.87 | 1,453 | | 0.97 | 1,544 |
| | 0.90 | 1,166 | | | |
| | 0.95 | 1,276 | 4 | 0.02 | 630 |
| | | | | 0.19 | 684 |
| | 0.02 | 571 | | 0.39 | 959 |
| 1 | 0.10 | 581 | | 0.47 | 887 |
| | 0.18 | 571 | | 0.57 | 1,098 |
| | 0.28 | 580 | | 0.68 | 1,092 |
| | 0.38 | 664 | | 0.76 | 1,301 |
| | 0.48 | 702 | | 0.87 | 1,237 |
| | 0.57 | 1,220 | | 0.94 | 1,289 |
| | 0.63 | 1,697 | | | |
| | 0.68 | 1,656 | 5 | 0 | 808 |
| | 0.72 | 2,026 | | 0.19 | 844 |
| | 0.77 | 2,044 | | 0.37 | 914 |
| | 0.81 | 2,313 | | 0.58 | 948 |
| | 0.84 | 1,846 | | 0.76 | 1,026 |
| | 0.89 | 2,174 | | 0.96 | 977 |
| | 0.95 | 2,540 | | | |
| | | | 6 | 0.02 | 891 |
| | 0 | 608 | | 0.06 | 898 |
| 2 | 0.004 | 581 | | 0.09 | 942 |
| | 0.14 | 668 | | 0.14 | 952 |
| | 0.16 | 592 | | 0.20 | 961 |
| | 0.30 | 599 | | 0.24 | 952 |
| | 0.45 | 1,010 | | 0.28 | 965 |
| | 0.55 | 1,168 | | 0.39 | 956 |
| | 0.65 | 1,642 | | 0.48 | 875 |
| | 0.71 | 1,384 | | 0.57 | 931 |
| | 0.75 | 1,758 | | 0.67 | 1,001 |
| | 0.80 | 1,371 | | 0.76 | 918 |
| | 0.86 | 1,885 | | 0.86 | 1,049 |
| | 0.90 | 1,904 | | | |
| | 0.94 | 1,978 | | | |

66

# APPENDIX B
# CHEMISTRY MODEL

## R. P. Rhodes

In order to calculate free-stream gas properties in a potentially reacting system from total pressure, static pressure, and gas compositon, the following assumptions were made:

1.  There is a unique relationship between elemental composition and total enthalpy. In this analysis, both gases were introduced near room temperature, where $H_T$ is 0 and all mixtures were assumed to have an $H_T$ of 0; $H_T$ is defined by:

$$H_T = \sum_i \left[ \beta_i \left( \int_{T_r}^{T} C_{P_i} \, dT + H_{f_r} \right) \right] + u^2/2 \qquad (B\text{-}1)$$

where

$\beta_i$ = Moles/g of species i

$C_{p_i}$ = Molar specific heat of species i

$T$ = Static temperature

$u$ = Velocity

$T_r$ = Reference temperature for the enthalpy

$H_f$ = Heat of formation of species i

2.  The state of reaction is known. Calculations were made assuming both frozen (unreacted) and equilibrium (completely reacted) gases.

3.  The compression process from the free stream to stagnation presure on the probe tip is isentropic and chemically frozen.

4.  Composition of air is assumed to be 0.2095 mole fraction $O_2$ and 0.7905 mole fraction $N_2$.

5.  The static pressure is assumed constant with duct radius and equal to the measured wall value.

6.  The gas mixtures are thermally perfect.

Given the pressure, enthalpy, and chemical composition, the computer program of Ref. 20 was used to calculate the gas properties. The program may be run assuming either frozen chemistry, in which case the species partial pressures are required, or equilibrium chemistry using the molar ratios of the elements.

The gas properties are calculated by the following procedure:

1.  From the mass fraction of elemental hydrogen, compute the moles/unit mass of each element,

$$\beta_H = \alpha_H / 1.008$$

$$\beta_O = 0.2095(1 - \alpha_H)/16 \tag{B-2}$$

$$\beta_N = 0.7905(1 - \alpha_H)/14.008$$

These variables are input to the gas properties program for the equilibrium calculation. For the frozen calculation, the partial pressures of $H_2$, $O_2$, and $N_2$ are required. For the gas constituents being considered, the moles/unit mass $(\beta)$ of the molecules is $\frac{1}{2}\beta$ of the element, and:

$$P_{p_i} = P\beta_i / \sum_i \beta_i \tag{B-3}$$

where is is each species.

2.  A velocity is assumed and the static enthalpy is calculated from:

$$H = H_T - v^2/2 \quad ; \tag{B-4}$$

3.  The remaining free-stream properties including entropy $(S_2)$ are calculated from the free-stream enthalpy, the measured static pressure, and composition using the gas properties program described in Ref. 18.

68

4.  An estimate of the total pressure is obtained from the isentropic relationship:

$$P_{T_1} = P\left(1 + \frac{\gamma-1}{2} M^2\right)^{\gamma/(\gamma-1)} \qquad \text{(B-5)}$$

using the Mach number and $\gamma$ from the calculations in Eq. (B-3). The entropy $(S_1)$ is then calculated using the gas properties program with frozen composition, $P_T$ from Eq. (B-5), and $H_T$. Since, for an adiabatic system,

$$P_{T_2}/P_{T_1} = \text{Exp}\ [-(S_2 - S_1)\, W/R_g] \qquad \text{(B-6)}$$

the total pressure $P_{T2}$ corresponding to the isentropic compression at $S_2$ may be obtained from Eq. (B-6).

5.  Steps 2 to 4 are repeated with a new value of u obtained from $(u_{new} - U_{old}) \sim (P_{T_{measured}} - P_{T_{old}})/(\rho u)_{old}$ until $(U_{new} - U_{old})$ is less than 1 ft/sec. The gas properties obtained in step 3 on the final iteration are taken to be the free-stream properties.

## NOMENCLATURE

A            Mass flow rate of air, lbm/sec

$B_\Phi$      Bias of the parameter ($\Phi$), units of $\Phi$

D            Duct diameter, 5.24 in.

F            Mass flow rate of fuel (hydrogen), lbm/sec

$F_H$         Hydrogen mass fraction, total hydrogen mass/total mass

f            Frequency, Hz

K            Coefficient of Kurtosis (Ref. 21)

Ku, Kv       Fringe spacing, ft x $10^{-6}$

$N_{Re}$      Reynolds number based on primary jet radius

P            Pressure, psia

$\Delta_P$    Difference between wall static pressure at station X and station zero, psf

R            Radius, in.

$R_g$         Universal gas constant 1,545 ft-lbf/lb-mole-$^\circ$R

S            Coefficient of skewness (Ref. 21)

$S_\Phi$      Precision index of the parameter ($\Phi$), units of $\Phi$

T            Temperature, $^\circ$R

$U_\Phi$      Uncertainty in the parameter ($\Phi$), units of $\Phi$

u            Mean axial velocity, ft/sec

u'           Root-mean-square fluctuating velocity, ft/sec

$u'/u_p$      Axial turbulence intensity

$\overline{u'v'}$     Shear stress correlation

W            Molecular weight of the mixture, lbm/mole

70

| v | Mean radial velocity, ft/sec |
|---|---|
| $v'$ | Root-mean-square fluctuating velocity, ft/sec |
| $v'/u_p$ | Radial turbulence intensity |
| X | Axial coordinate measured from primary nozzle exit location, in. |
| $X_{FS}$ | Axial location of the forward stagnation point on the duct wall (Fig. 1) |
| $X_{RS}$ | Axial location of the rear stagnation point on the duct wall (Fig. 1) |
| $a_H$ | Mass fraction of elemental hydrogen |
| $\beta_i$ | Parameter, moles/gm of species i |
| $\gamma$ | Ratio of specific heats |
| $\mu$ | Dynamic viscosity, lbm/ft-sec |
| $\xi$ | Measured parameter which defines $\Phi$ |
| $\rho$ | Density, lbm/ft$^3$ |
| $\Phi$ | Dummy parameter, scalar |

## Subscripts

| 1,2 | Arbitrary stations in iteration scheme |
|---|---|
| A | Argon |
| c | Centerline |
| D | Duct |
| H | Hydrogen |
| i | Arbitrary chemical species |
| N | Nitrogen |
| O | Oxygen |
| p | Primary jet property |

r   Reference value

s   Secondary

T   Total or stagnation conditions